Experimental Mechanics
https://doi.org/10.1007/s11340-024-01136-z

RESEARCH PAPER

An Inverse Parameter Identification in Finite Element Problems Using Machine Learning-Aided Optimization Framework

A. Tariq[1] · **B. Deliktaş**[1]

Received: 7 May 2024 / Accepted: 6 December 2024
© Society for Experimental Mechanics 2025

Abstract

Background The ability of finite element analysis to produce high fidelity results is greatly dependent on quality of constitutive model and the accuracy of their parameters. As such, the calibration of phenomenological constitutive models to replicate real-world behaviors has remained a focal point of many research works.

Objective A new inverse identification approach combining numerical-experimental methods and data-driven techniques to characterize the nonlinear response of materials using a single experiment is proposed.

Methods This approach integrates finite element analysis, optimization methods and machine learning techniques, such as Artificial Neural Networks and Support Vector Regression, to accurately determine model parameters while significantly reducing computational time. This approach can be used to characterize a wide range of models irrespective of the number of parameters involved. A detailed flowchart of the methodology focusing on its implementation aspects is provided and its each module is explained.

Results The proposed model calibration approach successfully identified eight parameters for a cohesive zone model implemented in user element subroutine (UEL), four parameters for a hardening model implemented in user material subroutine (UMAT), and five parameters for a Johnson–Cook plasticity model. In all cases, this method achieved an excellent fit between the simulation and experimental results. Moreover, it demonstrated a significant improvement in efficiency, being 2–3 times faster than traditional optimization algorithms in determining optimal parameters.

Conclusions Based on the presented investigations, the proposed machine learning-based inverse method can significantly accelerate the parameter identification procedure and can be extended to a wide range of material models.

Keywords Parameter identification · Constitutive model · Inverse method · Machine learning · Finite element analysis

Introduction

Finite element (FE) analysis stands as a cornerstone in engineering simulations, offering a powerful tool for predicting complex behaviors in various problems. However, ensuring the accuracy and reliability of these simulations heavily relies on robust material modeling. Engineers often encounter two key challenges when dealing with materials in their studies: selecting the most suitable constitutive model for a given problem and accurately determining the parameters for these models. The careful selection and calibration of constitutive models plays a critical role in predictive computational simulations, thus emphasizing their importance in engineering analyses.

The pursuit of more accurate models for the elasto-plastic behavior of metals has been a focal point in materials science and engineering. Various empirical and phenomenological models have been proposed over the years to capture the stress–strain curves accurately, particularly focusing on hardening phenomena. These models include well-known formulations such as the Hollomon equation [16], the Ludwik equation (Ludwik, 1909), the Voce equation [49], and the Estrin and Mecking model [11]. Additionally, more advanced and complex phenomenological models like the Johnson–Cook model [17] and its modified versions (Wang, 2013 [13],), Power Laws, and strain-path dependent models

✉ A. Tariq
aimantariq@uludag.edu.tr

B. Deliktaş
bdeliktas@uludag.edu.tr

[1] Department of Civil Engineering, Artificial Intelligence and Computational Mechanics Laboratory, Bursa Uludag University, Gorukle Campus, 16059 Bursa, Turkey

Published online: 16 January 2025

have been proposed. Furthermore, thermo-elasto-viscoplastic constitutive models have been developed to capture the thermo-mechanical behavior of metals comprehensively, considering factors such as material behavior, temperature, strain range and strain rate [20, 46].

The complexity of constitutive models, coupled with the increasing demand for higher fidelity in simulations, often necessitates a laborious calibration process involving multiple experimental campaigns. For instance, calibrating parameters for models like the Johnson–Cook model requires a series of quasi-static tests on standard strength testing machines to determine constants such as A, B, and n, while dynamic tests are needed to obtain the value of the strain rate sensitivity index. Similarly, the yield criterion Yld2000 [2] relies on eight material parameters, necessitating multiple tests including three uniaxial yield stress tests, three uniaxial anisotropy coefficient tests, and tests for bi-axial yield stress and anisotropy coefficient determination. These experiments are time-consuming, intricate, and demand specialized equipment. Hence, there exists a need for model calibration processes capable of expediting experimental campaigns while preserving the accuracy of the models.

According to Pierron and Grédiac [33], there is a notable surge in research aimed at reducing the reliance on traditional mechanical tests by utilizing a combination of inverse methodologies, heterogeneous tests, and full-field measurements, often referred to as Material Testing 2.0. The inverse method specifically focuses on identifying parameters of constitutive model using boundary conditions such as measured force and displacements. In computational mechanics, the development of inverse methods has progressed rapidly in recent years, resulting in various approaches based on full-field measurements. Examples include the methodologies proposed by Prates et al. [36], Markiewicz et al. [25], and Bonnet (2005). An illustrative instance of an inverse method is introduced by Pottier et al. [35] for estimating the inelastic heat fraction. Their approach involved utilizing full-field measurement techniques to capture comprehensive displacement/strain maps at the surface of a specimen during heterogeneous tests, along with temperature measurements.

Various inverse methods have been developed for parameter identification in the field of solid mechanics, such as Finite Element Model Updating (FEMU) [19], Virtual Fields Method (VFM) [14], Equilibrium Gap Method (EGM) [8], Constitutive Equation Gap Method (CEGM) [21], Integrated Digital Image Correlation Method (Integrated-DIC) [38], Dissipation Gap Method (DGM) [3], Self-Optimizing Method (Self-OPTIM) [51], and Constitutive Compatibility Method (CCM)) [29]. These methods have demonstrated effectiveness in determining parameters of both linear and non-linear constitutive models, particularly in plasticity and viscoplasticity. Applications of these strategies can be found in studies such as those by Andrade-Campos et al. [1], Martins et al. [28], and Chemisky et al. [7]. These inverse method strategies have demonstrated considerable effectiveness in identifying parameters of both linear and non-linear constitutive models, particularly in the field of plasticity and viscoplasticity. Other inverse methods utilized for determining the parameters of a FE model include those outlined by Fayad et al. [12], Nsengiyumva and Kim [30], Makhool and Balzani [24], Sun et al. [45]. Springmann and Kuna [44] employed inverse methodology with gradient-based optimization algorithm to identify the parameters for the Gurson-Tvergaard-Needleman model applied to StE 690 structural steel. Additionally, inverse analysis has been widely used for fitting damage models as well. Cooreman et al. [9] employed an enhanced meta-modeling technique to identify parameters related to a Hill 1948 yield and failure surface and parameters for Swift hardening. Similarly, [39, 40]focused on hardening and damage models for sheet metal, emphasizing optimization techniques and difficulties involved in model fitting.

The primary challenge with many existing inverse strategies is their reliance on full-field measurements across the whole specimen domain, that can be impractical for certain applications. This is especially true in cases where through-thickness assumptions, such as plane stress conditions, do not hold, necessitating internal measurements that are difficult to acquire. Computed tomography (CT) scans offer a potential solution to this issue by measuring the full-field volumetric displacements, but it has a drawback of requiring costly equipment. Additionally, interpreting full-field measurements from different experiments is complex due to uncertainties associated with Digital Image Correlation (DIC), currently the most feasible method for gathering such displacement measurements. Furthermore, some inverse methods require a significant number of finite element simulations conducted iteratively, resulting in high computational costs and time constraints. Certain inverse methods necessitate users to preselect a constitutive model before initiating the iterative search process. As a consequence, the energy required in these methods would be multiplied by the number of constitutive models the researcher wishes to evaluate, presenting challenges in material model selection.

In this study, a new inverse methodology that employs a hybrid experimental–numerical scheme for effectively calibrating constitutive models is introduced. Unlike traditional inverse methods, this approach integrates FE analysis and optimization techniques with Machine Learning (ML) methods, including Artificial Neural Networks (ANN) and Support Vector Regression (SVR), to determine the constitutive model parameters accurately and reduce the overall computation time. Notably, this methodology can be used for fitting various models, such as hardening and damage models, as well as other user subroutine models, irrespective

of the number of parameters involved. This model calibration framework is termed SmartFIT in the rest of the paper. To illustrate the efficiency of SmartFIT, its application has been demonstrated in three distinct cases: the cohesive zone model implemented in UEL, a hardening model implemented in UMAT, and the Johnson–Cook plasticity model. Additionally, a realistic structural analysis with complex loading conditions involving a beam-column connection under cyclic loading is conducted to illustrate the efficiency of this framework. To further evaluate the effectiveness of SmartFIT, its overall analysis time and computational accuracy is compared with those of a traditional optimization algorithm.

Currently, the development of the user interface for the proposed methodology aimed at facilitating the implementation of new problems is in progress. This user interface is being built within the Python environment, leveraging open-source libraries for machine learning, optimization algorithms and to establish a connection between Python and Abaqus. This interface will make it more practical for practitioners from different fields to determine model parameters automatically and efficiently.

Inverse Method for Parameter Identification

Assume a continuum solid body occupying the domain Φ, bounded by $\partial\Phi$ and the material within this domain to be homogeneous as shown in Fig. 1. The boundary conditions in this domain consists of $\mathcal{B}_f$ and $\mathcal{B}_u$ boundaries, so that, $\partial\Phi = \mathcal{B}_f \cup \mathcal{B}_u$ and $\mathcal{B}_f \cap \mathcal{B}_u = \phi$.

The mechanical state of Φ can be described by three differential equations when infinitesimally small displacements, static equilibrium and linear elastic behavior of a body is assumed and forces acting on the body are neglected. The equations are,

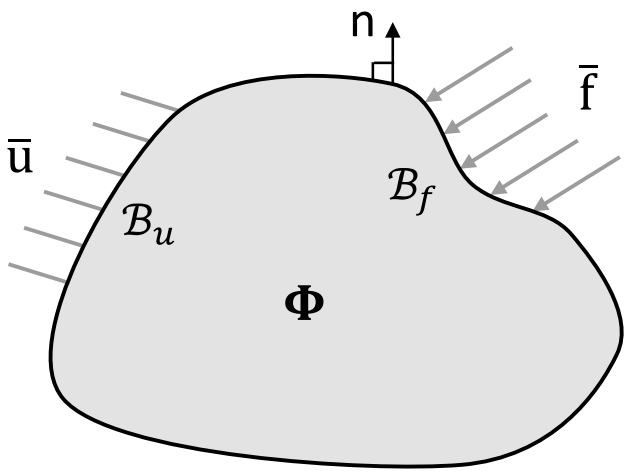


Fig. 1 A continuum solid body with prescribed force and displacement boundary condition

a) the classical equilibrium equations obtained from the equilibrium of forces,

$$\begin{aligned} div\sigma &= 0 \quad in\,\Phi \\ \sigma.\mathrm{n} &= \bar{f} \quad on\,\mathcal{B}_f \end{aligned} \tag{1}$$

b) the kinematic compatibility equations

$$\begin{aligned} \varepsilon &= \tfrac{1}{2}\left(\nabla u(x) + \nabla^T u(x)\right) \quad in\,\Phi \\ \mathrm{u} &= \bar{u} \quad on\,\mathcal{B}_u \end{aligned} \tag{2}$$

c) the constitutive equations

$$\sigma = C : \varepsilon \quad in\,\Phi \tag{3}$$

Here, σ denotes the Cauchy stress, $\bar{f}$ denotes the traction field prescribed over $\mathcal{B}_f$, u denotes the displacement field, $\bar{u}$ denotes the displacement field prescribed over $\mathcal{B}_u$, ε denotes the strain tensor, and n denotes the outward unit normal to $\partial\Phi$. The relationship between stress and strain is described using Eq. (3), where C represents the constitutive material tensor. In isotropic linear elastic material behavior, $C(\wp)$ corresponds to the Hooke's equation, such that $\wp$ includes two essential parameters: Young's modulus (E) and Poisson's ratio (ν).

In the forward method-based problems, material parameters ($\wp$), boundary conditions ($\bar{f}$ and $\bar{u}$) and the geometry of the body are known before conducting (FE) simulations. The output of these simulations typically comprises displacements, strains, and stresses, all of which must satisfy Eqs. (1), (2), and (3). However, in practical scenarios, the parameters governing a constitutive model are often initially unknown and only the boundary conditions ($\bar{f}$ and $\bar{u}$) and measured displacement field ($\hat{u}$) are known. These unknown constitutive model parameters are determined through the application of inverse methods, representing a pivotal technique in solid mechanics. The $\hat{u}$ can be acquired using non-contact measurement techniques like DIC. Subsequently, the strain field necessary for computing the stresses are determined with Eq. (2). A comparison between forward and inverse methodologies is depicted in Fig. 2.

In solid mechanics, the accuracy of finite element (FE) simulations relies greatly on the constitutive material model employed which, in turn, relies on the values of various parameters involved [34]. A common method for determining the parameters of a constitutive model through an inverse method, involves minimizing a function $\mathcal{L}$ that calculates the difference between the experimentally observed material behavior and the mathematical model selected to reproduce it,

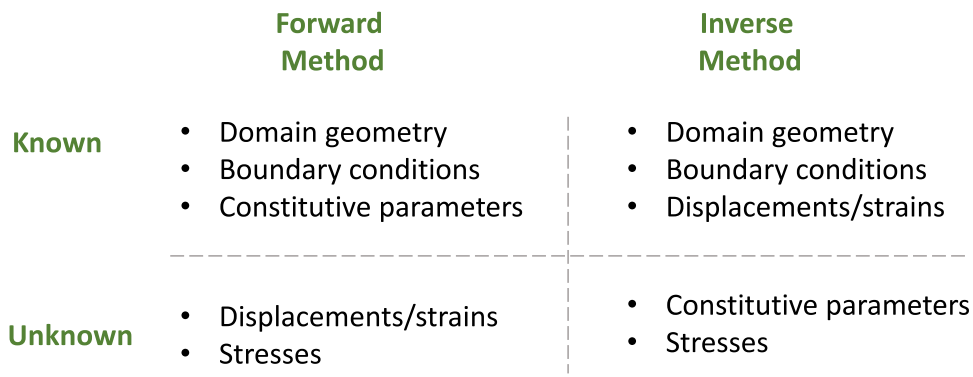


Fig. 2 Comparison of forward and inverse method

$$\min f = \mathcal{L}(\wp, \phi^{\text{num}}, \phi^{\text{exp}}) \quad \text{subject to} \quad \begin{cases} g(\wp, \phi^{\text{num}}, \phi^{\text{exp}}) \leq 0, \\ \wp_{\min} \leq \wp \leq \wp_{\max}, \\ K(\wp)u = F \end{cases} \tag{4}$$

In this formulation, $\wp$ denotes the list of parameters to be determined, ϕ denotes the measured properties, e.g., displacement or strain. The superscripts "*num*" and "*exp*" denote numerically computed and experimental values, respectively. Function g defines the set of functions serving as inequality constraints during optimization. Additionally, $\wp_{min}$ and $\wp_{max}$ are the parameter bounds denoting the maximum and minimum values for each variable. An equality constraint Ku = F can be established, typically fulfilled when employing finite element analysis (FEA) or other static equilibrium conditions.

Proposed Machine Learning Based Inverse Methodology

In this section, a hybrid experimental–numerical scheme designed to leverage machine learning (ML) techniques and optimization algorithms for determining the parameters of a constitutive model in finite element (FE) problems is introduced. The proposed inverse methodology referred to as SmartFIT, integrates FEA using Abaqus with ML techniques such as Artificial Neural Networks (ANN) and Support Vector Regression (SVR), along with advanced optimization methods. This model calibration tool ensures that the numerical results obtained from FE analysis align accurately with experimental data. This approach significantly reduces the number of expensive FE simulations typically required to accurately fit an experimental curve. The overall parameter identification procedure facilitated by SmartFIT is depicted in Fig. 3. This figure provides a visual representation of the integration between experimental data, FEA, ML techniques, and optimization methods employed.

Features Sampling Technique for Design of Experiment

Once the problem to be solved is defined, the initial step involves conducting a design of experiments (DoE) to effectively characterize the multi-dimensional space of parameters using FE attributes. This process, as illustrated in Fig. 3, deals with identifying various types of FE attributes based on the parameters targeted for optimization. These attributes encompass geometric attributes, element property attributes, material property attributes, and boundary conditions attributes. For instance, material property attributes of the problem may include parameters such as Young's modulus, Poisson ratio, yield stress, strain hardening exponent, and damage variables. Element property attributes can be cohesive strength in normal and tangential directions, the number of integration points. Boundary conditions attributes can be applied forces and strains across different components of the system.

After these attributes for the problem are identified, they collectively constitute a list of input design parameters (χ), represented as:

$$\chi = \left[\mathcal{A}_1 \mathcal{A}_2 \mathcal{A}_3 \cdots \mathcal{A}_n\right] \tag{5}$$

where, n signifies the total number of input design parameters for the optimization. Subsequently, upper and lower bounds are assigned to these attributes to ensure that optimal values lie within their respective limits. The upper limit of the input design parameter comprises the maximum values of the attributes, while the lower limit contains the minimum values.

$$\begin{aligned} \chi_{up} &= [\mathcal{A}_{1_{max}}, \mathcal{A}_{2_{max}}, \mathcal{A}_{3_{max}}, \ldots, \mathcal{A}_{n_{max}}] \\ \chi_{low} &= [\mathcal{A}_{1_{min}}, \mathcal{A}_{2_{min}}, \mathcal{A}_{3_{min}}, \ldots, \mathcal{A}_{n_{min}}] \end{aligned} \tag{6}$$

The next step after determining the input design parameters and assigning their corresponding limits involves employing DoE techniques to systematically search the

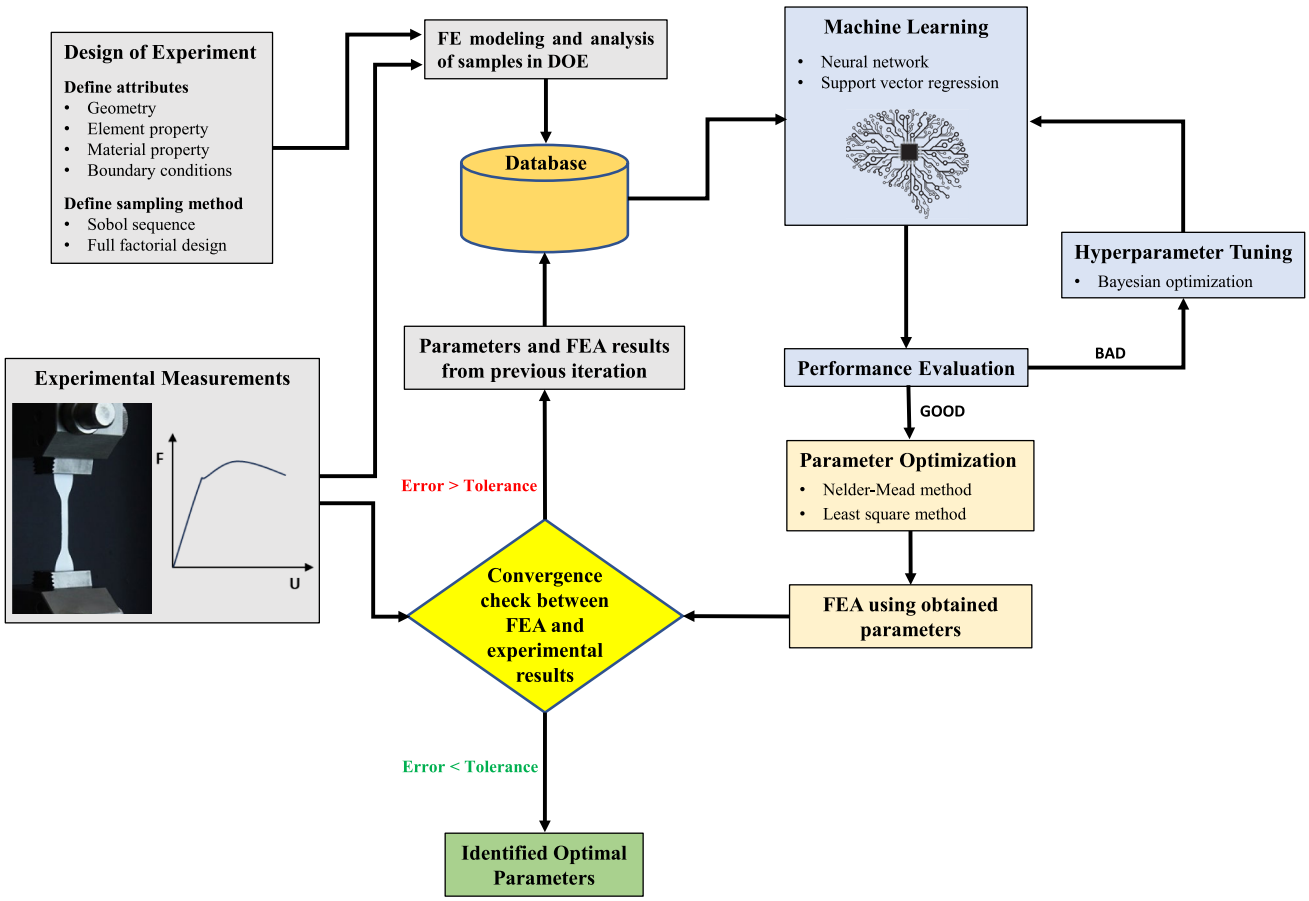


Fig. 3 The overall workflow of the methodology implemented in SmartFIT

parameter space domain. To ensure thorough coverage of the input parameters' domain without any preconceived biases, it is advisable to utilize space-filling designs, such as those proposed by Lin et al. [22]. These designs treat various regions of the input parameters' domain with equal importance. Conventional random and stratified sampling methods, as highlighted by Burhenne et al. [5], may result in clusters of data points or leave gaps in the parameter space. Santiago et al. [43] conducted a comprehensive review of various space-filling techniques such as low good lattice points, Latin hypercube sampling and discrepancy sequences. Through their comparative analysis, they found that the Sobol sequence stands out as an effective choice due to its ability of maintaining good balance between random distribution and regular grid method.

Sobol sequence sampling [41] is categorized within the family of quasi-random sampling techniques, also referred to as low-discrepancy sequences. These sampling methods are widely employed for sensitivity analyses. The Sobol sampling method distributes multiple parameters as uniformly as possible across the multidimensional parameter space, as indicated by Renardy et al. [37], Saltelli et al. [41], and Dige and Diwekar [10]. The key distinguishing feature of Sobol sequence sampling is its ability to select sample values while taking into account previously sampled points. This approach helps prevent the formation of clusters and gaps within the sampled data, even when using a subset of the entire dataset [5]. This characteristic enhances the efficiency and effectiveness of the sampling process, contributing to more robust and comprehensive analyses.

Sobol sequence sampling method is incorporated in SmartFIT and necessitates the specification of upper and lower bounds for each parameter. Typically, these bounds are determined either through engineering intuition or by referencing the maximum and minimum values documented in literature. During the optimization process, these bounds serve as constraints to ensure that the optimal parameter values fall within their specified ranges. An example illustrating the sampling of the bounded parameter space using a Sobol sequence is provided in this paper. The distribution of eight pairs of parameters as depicted later in Fig. 7, demonstrating a well-dispersed arrangement across the multidimensional parameter space.

Another sampling method available in SmartFIT is the full factorial design. In this approach, upper and lower bounds are specified for each parameter. The full factorial design of experiments method systematically evaluates the response for every possible combination of parameter levels using the specified bounds. The total number of samples collected using a full factorial design is determined by the formula L^P, where L represents the number of levels examined (associated with the number of bounds), and P represents the number of parameters. For instance, if four parameters need to be optimized with two levels (upper and lower bounds), employing a full factorial design would result in a total of 16 samples. However, it's important to note that as the number of parameters increases, the number of samples in the design of experiments increases exponentially. Consequently, due to the computationally expensive nature of this methodology, it is advisable to utilize full factorial design only when the number of parameters to be identified is relatively small. Otherwise, Sobol sampling is preferred due to its ability to efficiently explore the parameter space without requiring exhaustive sampling of all possible combinations.

Finite Element Analyses

The second crucial step in SmartFIT involves conducting FEA to generate a database encompassing the responses of interest for each set of design parameter samples within the DoE. The response of interest in the examples provided in this study is the nonlinear force versus displacement curve, although this may vary depending on the specific problem under consideration. To accomplish this, the FE model of the problem according to the experimental conditions is created within the ABAQUS software, and its input file (.inp) is obtained. Subsequently, SmartFIT operates by accessing the input file of the model, assigning a set of design parameters from the sampling method, and then executing the modified input file utilizing ABAQUS as the backend solver. Once the simulations for all the samples are completed, SmartFIT reads the output files (.odb) and organizes the simulation results corresponding to each set of design parameter sample. These results form a database that includes samples of constitutive model parameters as input features and the corresponding FE simulation results such as force–displacement responses as the output data. This comprehensive dataset is utilized as the training data for the subsequent ML algorithms. SmartFIT seamlessly interacts with the ABAQUS software throughout the entire process, from preprocessing and executing the simulations to post-processing the results without the need for human intervention.

Machine Learning

Once the database is complete, the next crucial step involves constructing a machine learning model that is capable of accurately capturing the influence of DoE attributes on the response of interest. Presently, SmartFIT offers two potent machine learning methodologies: artificial neural networks (ANN) and support vector regression (SVR). These models are built leveraging the Keras and scikit-learn open-source machine learning libraries within the Python environment. Both ANN and SVR models have demonstrated high accuracy in predicting multiple output values in regression problems [48]. However, to achieve optimal performance, numerous hyperparameters for each model need to be fine-tuned. For instance, ANNs necessitate specification of parameters such as the number of hidden layers, the number of neurons in each layer, the choice of activation function, and the learning rate. On the other hand, SVRs require parameters including kernel type, regularization parameter, and epsilon. Traditionally, hyperparameter tuning has been conducted manually through trial-and-error method, random search method and grid search method particularly for smaller databases and standalone modeling studies. However, to streamline this process and obtain the optimal hyperparameters automatically, SmartFIT incorporates an advanced optimization technique known as Bayesian optimization. Bayesian optimization utilizes a 'surrogate' model, such as ANN or SVR, to navigate the parameter space and converge upon a combination of parameter values that yield the best cross-validation performance. This approach accelerates the achievement of optimal model configurations.

Moreover, SmartFIT is equipped with data preprocessing modules that offer versatile functionalities. These modules facilitate scaling of both input features and targets within the dataset to a uniform range between 0 and 1. Additionally, they enable partitioning of the dataset, allocating 90% of the overall data for training and reserving 10% for testing purposes. Furthermore, the modules measure the error between the predicted and actual values using various performance metrics, providing a comprehensive evaluation of model performance.

Optimization Procedure

A ML model can be considered as a versatile black box function capable of approximating complex nonlinear relationships. After the ML model is trained and tested to ensure accuracy it is integrated into an objective function aimed at minimizing the difference between target and predicted output using the least squares method. This can be formulated as

$$min \sum \left(\frac{y_i - \hat{y}_i}{y_i} \right)^2, \quad where\ \hat{y}_i = ML(\mathcal{A}_1, \mathcal{A}_2, \mathcal{A}_3, \ldots, \mathcal{A}_n) \tag{7}$$

where, y_i and $\hat{y}_i$ are the target and the predicted values for the i^{th} data point. The optimization process revolves around the minimization of this objective function. To facilitate this, SmartFIT automatically selects upper and lower bounds for each parameter based on the maximum and minimum values observed within the DoE. Among the various choices of optimization methods available, SmartFIT employs the Nelder-Mead method due to its robustness and widespread applicability. The Nelder-Mead method is renowned for its versatility in optimizing both one-dimensional and multidimensional functions with numerical inputs, making it well-suited for problems where the gradient of the function is unknown or challenging to compute. Using a pattern search optimization algorithm, the Nelder-Mead method systematically adjusts parameter values within the finite element model to iteratively converge towards the optimal solution.

Upon acquiring the optimal parameter values, they are implemented into the FE model input file. This modified input file is then passed over to the Abaqus solver to carry out simulations. If the difference between the results obtained from the new FE analysis and the experimental data exceeds a predefined tolerance threshold, the obtained parameters along with the FE output are appended to the database. Subsequently, the ML model is retrained using the new dataset which includes the current iteration. By continually adjusting parameters and enhancing the ML model, SmartFIT progressively improves the accuracy of its FE predictions. This iterative cycle continues until the simulation results align accurately with experimental results. This process ensures that the model accurately represents the physical system under investigation.

Parameter Identification Using SmartFIT

To demonstrate the effectiveness of the SmartFIT model calibration framework, three distinct computational examples are analyzed. These examples serve as test cases, each targeting specific constitutive models and element behaviors. The first computational example involves a patch test aimed at calibrating a cohesive zone model implemented through user-defined element (UEL) subroutines. Within this context, the objective is to identify 8 parameters governing the traction–separation response of the cohesive zone model.

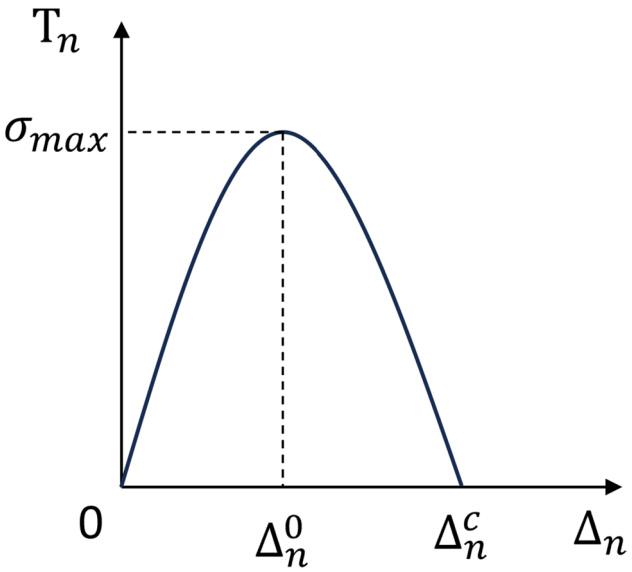


Fig. 4 Traction–separation response using PPR model. (mode I)

This process involves precisely characterizing the behavior of cohesive materials under varying loading conditions. The second example involves a compact tension test, leveraging the User Material (UMAT) subroutine. Here, the focus is on identifying four critical parameters essential for defining the isotropic power-law hardening plasticity model that represents actual material behavior. This model facilitates the simulation of plastic deformation under complex loading scenarios. The final computational example involves a tensile test employing the classic Johnson–Cook model. In this context, the objective is to identify five parameters governing the elastic and plastic response of the material. The Johnson–Cook model is renowned for its versatility in capturing material behavior, making accurate parameter identification crucial for reliable simulations. By examining these computational examples, the SmartFIT optimization framework is thoroughly evaluated.

Application 1—UEL Implementation of Cohesive Zone Model

Theoretical Background

The cohesive zone model utilized in this example to simulate the traction–separation response is derived from the PPR potential-based model introduced by Park and Paulino, [31],Park et al., [32]. This model's potential is formulated as:

$$\Psi = (\Delta_n, \Delta_t) = \min(\phi_n, \phi_t) + \left[\Gamma_n \left(1 - \frac{\Delta_n}{\Delta_n^c} \right)^a \left(\frac{m}{a} + \frac{\Delta_n}{\Delta_n^c} \right)^m + \langle \phi_n - \phi_t \rangle \right] \times \left[\Gamma_t \left(1 - \frac{|\Delta_t|}{\Delta_t^c} \right)^\beta \left(\frac{n}{\beta} + \frac{|\Delta_t|}{\Delta_t^c} \right)^n + \langle \phi_t - \phi_n \rangle \right] \tag{8}$$

In this context, ϕ_t and ϕ_n denotes the tangential and normal cohesive energy. $a(a > 1)$ and $\beta(\beta > 1)$ are the shape parameters to regulate the traction–separation curve shape. Δ_t^c and Δ_n^c represent the critical displacement of the tangential and normal separation Δ_t and Δ_n, as depicted in Fig. 4. Additionally, Γ_t and Γ_n represents energy constants that are interconnected with shape parameters, cohesive energy, and initial slope parameters m and n.

Within the PPR model, the normal traction is computed by differentiating the potential with respect to the normal separation, expressed as:

$$T_n(\Delta_n,\Delta_t)=\frac{\Gamma_n}{\Delta_n^c}\left[m\left(1-\frac{\Delta_n}{\Delta_n^c}\right)^a\left(\frac{m}{a}+\frac{\Delta_n}{\Delta_n^c}\right)^{m-1}-a\left(1-\frac{\Delta_n}{\Delta_n^c}\right)^{a-1}\left(\frac{m}{a}+\frac{\Delta_n}{\Delta_n^c}\right)^m\right]\times\left[\Gamma_t\left(1-\frac{|\Delta_t|}{\Delta_t^c}\right)^\beta\left(\frac{n}{\beta}+\frac{|\Delta_t|}{\Delta_t^c}\right)^n+\langle\phi_t-\phi_n\rangle\right] \quad (9)$$

As per Park and Paulino [31], the expression for the normal critical displacement Δ_n^c is formulated as:

$$\Delta_n^c=\frac{\phi_n}{\sigma_{max}}a\lambda_n(1-\lambda_n)^{a-1}\left(\frac{a}{m}+1\right)\left(\frac{a}{m}\lambda_n+1\right)^{m-1} \quad (10)$$

The initial slope parameter m is defined as:

$$m=\frac{a(a-1)\lambda_n^2}{(1-a\lambda_n^2)} \quad (11)$$

Here, the initial slope indicator λ_n is represented as $\lambda_n=\Delta_n^0/\Delta_n^c$. Additionally, the normal cohesive energy corresponds to the area enclosed by the abscissa and the curve in Fig. 4.

$$\phi_n=\int_0^{\Delta_n^c}T_n(\Delta_n,0)d\Delta_n \quad (12)$$

Combining Eq. (12), the cohesive energy ϕ_n can be directly derived from the cohesive strength σ_{max} and the normal critical displacement Δ_n^c.

$$\phi_n=\frac{\sigma_{max}\Delta_n^c}{a\lambda_n(1-\lambda_n)^{a-1}\left(\frac{a}{m}+1\right)\left(\frac{a}{m}\lambda_n+1\right)^{m-1}} \quad (13)$$

Given the monotonic relationship between the initial slope indicator λ_n and the initial slope parameter m, λ_n can be reformulated as:

$$\lambda_n=\sqrt{\frac{m}{a(m+a-1)}} \quad (14)$$

It's important to highlight that the shape parameters a and β solely control the concavity or convexity of the traction–separation curve. When both a and β fall within the range $1 < a, \beta < 2$, the traction–separation curve exhibits a concave shape. Conversely, if a and β exceed 2 $(a, \beta > 2)$, the curve appears convex. Notably, when if a and β are approximately equal to 2 $(a, \beta \approx 2)$, the softening phase of the curve closely resembles a straight line, as depicted in Fig. 5.

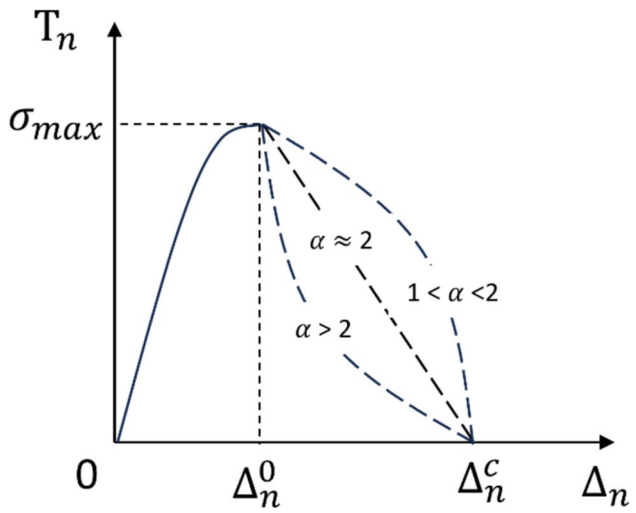


Fig. 5 Traction–separation curve for various values of shape parameter (α) (mode I)

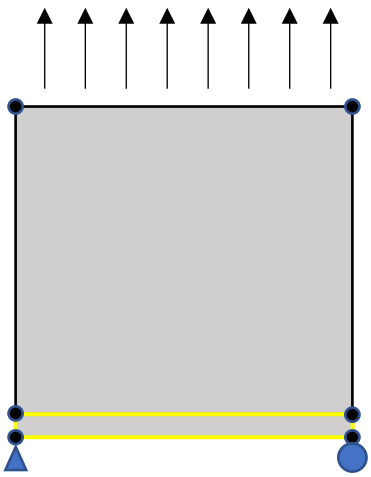


Fig. 6 Geometry of the model with cohesive element

Problem Definition

A square plate, measuring 0.1 mm by 0.1 mm, is subjected to uniaxial loading in the vertical direction. This loading is achieved by imposing a displacement of up to 0.03 mm at the nodes along the upper edge of the plate. The specimen is represented using a single continuum quadratic plane stress element comprising 4 nodes. Additionally, a cohesive element is integrated at the bottom of the plate, as illustrated in Fig. 6. Linear elastic behavior is assumed for the plate material, characterized by a Young's modulus of 32 GPa and a Poisson's ratio of 0.2. These properties provide fundamental parameters governing the response of the plate to the applied loading conditions.

The cohesive zone model that is essential for simulating the traction–separation behavior, is derived using the PPR potential-based model outlined in Sect. "Theoretical Background". This cohesive zone model is integrated into ABAQUS as a user-defined element (UEL) subroutine, necessitating the accurate definition of 8 parameters. These parameters include the normal and tangential fracture energies (ϕ_n and ϕ_t), normal and tangential cohesive strengths (σ_{max} and τ_{max}), shape parameters (α and β), as well as the normal and tangential initial slope indicators (λ_n and λ_t). To determine these parameters effectively, the stress-displacement curve provided by Park and Paulino [31] serves as a reference curve within SmartFIT.

To initiate the optimization process for these parameters, the first crucial step is to generate a sufficient number of samples using the design of experiments methodology. In this regard, the Sobol sampling method is employed to

Table 1 Upper and lower bound of PPR model parameters

Parameters	Min. Value	Max. Value
Normal fracture energy ($\boldsymbol{\phi_n}$)	0.07	0.4
Tangential fracture energy ($\boldsymbol{\phi_t}$)	0.07	0.4
Normal cohesive strength ($\boldsymbol{\sigma_{max}}$)	1	5
Tangential cohesive strength ($\boldsymbol{\tau_{max}}$)	1	6
Normal shape parameter ($\boldsymbol{\alpha}$)	2.1	6
Tangential shape parameter ($\boldsymbol{\beta}$)	1.1	3
Normal initial slope indicator ($\boldsymbol{\lambda_n}$)	0.001	0.008
Tangential initial slope indicator ($\boldsymbol{\lambda_t}$)	0.001	0.008

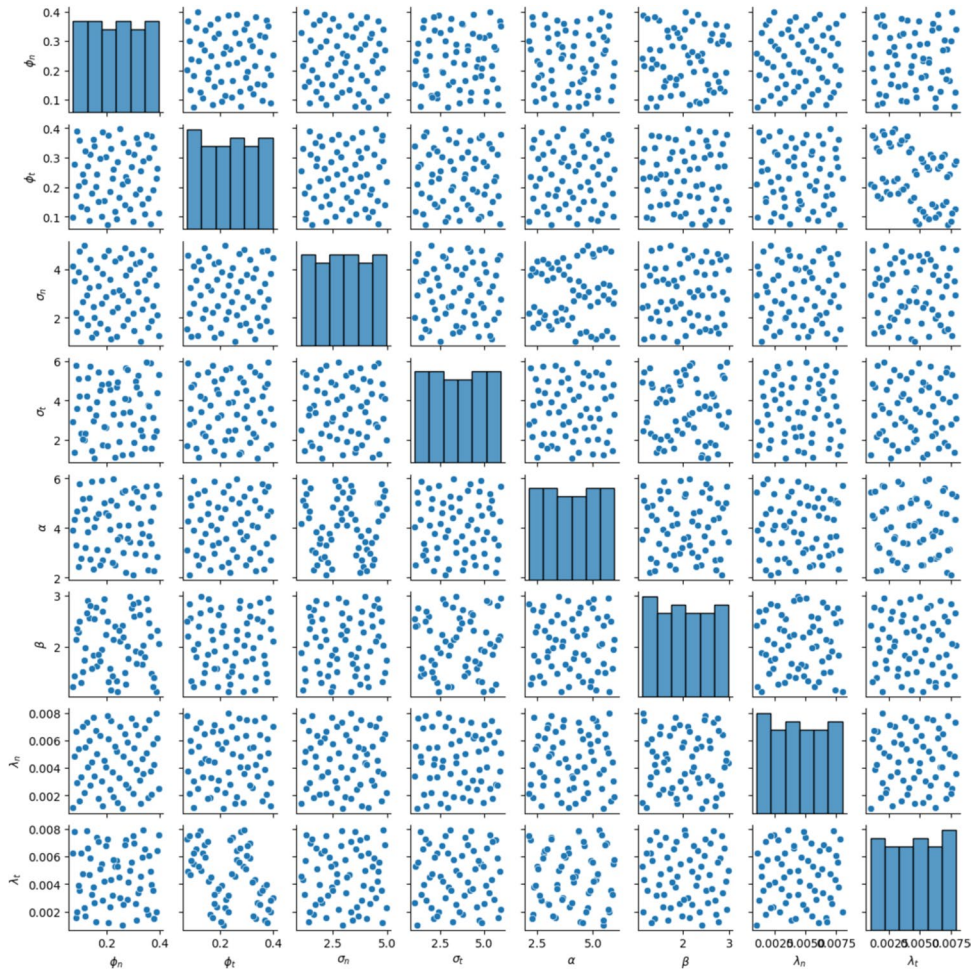


Fig. 7 Pairs plot for the samples in DOE

generate 64 samples. This method allows for a systematic and efficient exploration of the parameter space after defining the minimum and maximum values for each parameter, as detailed in Table 1. In the SmartFIT methodology, 64 samples are typically used for parameter identification when dealing with identification of more than five parameters. Although this sample size is usually sufficient, it can be adjusted depending on the complexity of the problem and the specific requirements of the analysis.

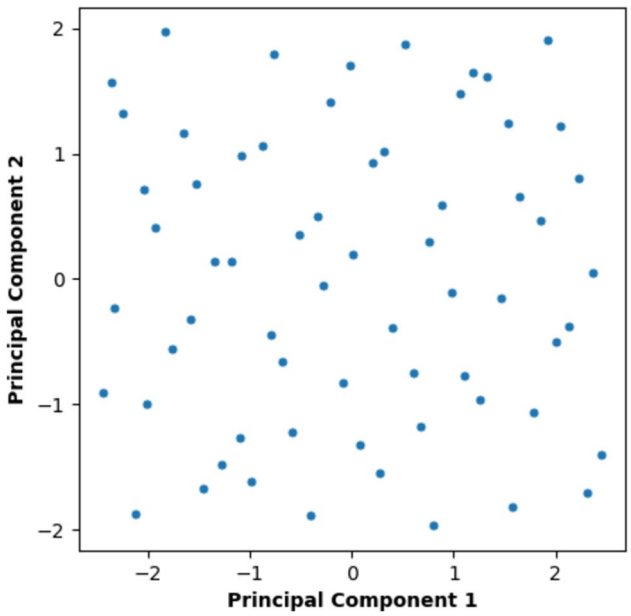
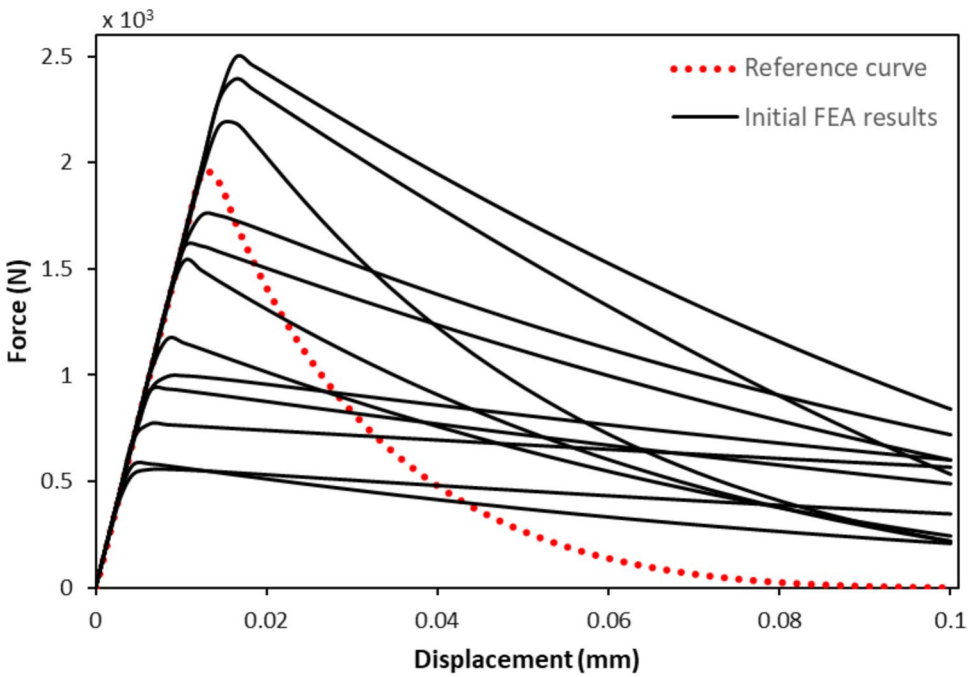


Fig. 8 Scatterplot after PCA reduction to 2-dimensions

The pairwise relationships among all parameter samples generated in the Design of Experiments (DOE) are depicted in Fig. 7. This figure visually represents a key characteristic of the Sobol sequence method i.e., a uniform spreading of sample points across the input parameter space, accompanied by non-overlapping projections. Moreover, a discrepancy value of 0.016 is computed for all samples utilizing the Sobol sequence method. This low discrepancy value indicates that the sample points are distributed quite evenly across the space, with only minor instances of empty areas or gaps. This observation suggests that the sampling strategy effectively covers the parameter space, facilitating a comprehensive exploration during the optimization process.

Principal Component Analysis (PCA) is utilized to examine the distribution of the overall dataset within a two-dimensional space. PCA is an unsupervised linear dimensionality reduction and data visualization technique tailored for handling complex high-dimensional datasets. The fundamental concept behind PCA involves reducing the dimensionality of highly correlated data by transforming the original set of vectors into a new set known as principal components. By doing so, PCA aims to capture the essence of the dataset while preserving its global structure. However, it's important to note that during this transformation process, local structures within the data may be lost. The PCA reduction of the 8-dimensional dataset to 2 dimensions is depicted in Fig. 8. This visual representation demonstrates that there are no visible overlaps or clusters of data points, indicating a relatively uniform distribution of data within the reduced two-dimensional space.

Fig. 9 Comparison of reference force–displacement curve with initial FEA results based on DoE



A finite element analysis of the model was conducted in Abaqus for each sample generated in the DOE. The resulting FE output data corresponding to each sample was then stored in the database for further analysis. Some of these FE results along with their comparison to the reference curve are illustrated in Fig. 9. Due to the inaccurate parameter values, the FE results deviate significantly from the reference curve. Once the data is obtained and preprocessing steps are completed, SmartFIT initiates the training of a machine learning (ML) model. This training process continues iteratively until the predictive performance of the model reaches a satisfactory level. To expedite the process of finding the best model hyperparameters, Bayesian optimization is employed. This optimization technique helps accelerate the search for optimal hyperparameters of the ML model. Once the model is trained well, it is integrated into the objective function of an optimization algorithm. This enables the determination of optimal parameters, as described in Sect. "Proposed Machine Learning Based Inverse Methodology", aiming to minimize the discrepancy between the FE results and the reference curve.

Optimization Results

At the end of each iteration within the SmartFIT framework, the optimal values determined through the optimization algorithm are applied to conduct a FEA, subsequently computing the force–displacement curve. If the calculated error between the reference and numerical curve exceeds the predefined tolerance threshold, the next iteration is initiated to further refine the parameter estimation process. As illustrated in Fig. 10, a total of 28 iterations were required to achieve convergence, where the error fell below the predefined tolerance level. A pattern in the error values was noticed as the iterations progressed. Specifically, following the fourth iteration, a consistent trend of gradual error reduction is observed with each subsequent iteration. This systematic decrease in error underscores the iterative refinement process within the framework, indicating a steady improvement towards achieving convergence and optimizing the parameter values effectively. The parameters obtained at the end of 28th iteration is presented in Table 2. A finite element analysis is then conducted utilizing these optimal parameters to check their alignment with the reference curve. The results from the finite element analysis and the reference curve are compared in Fig. 11, revealing a perfect

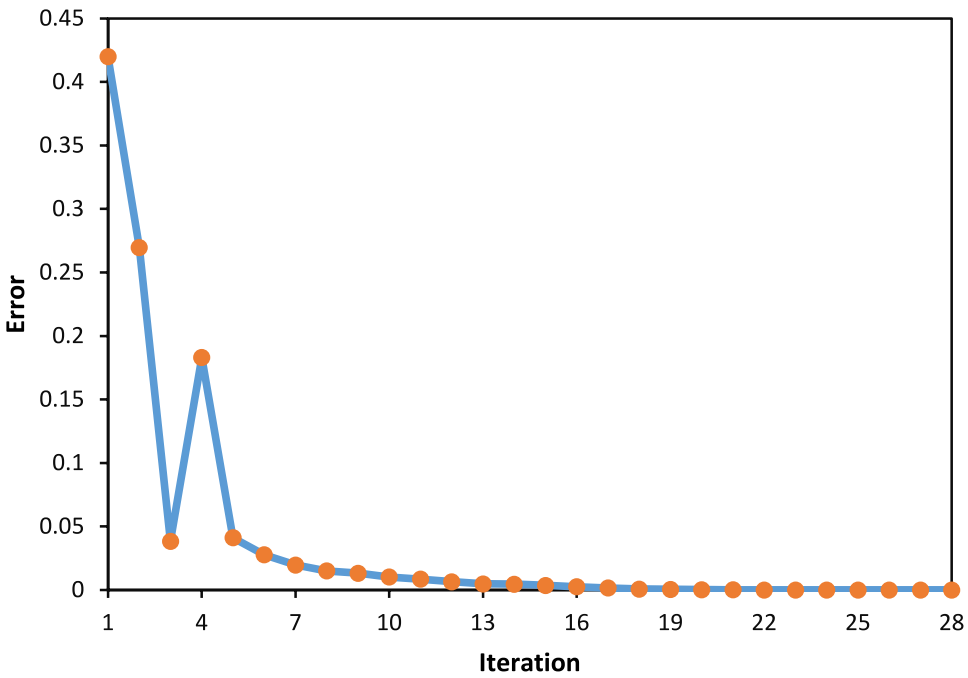


Fig. 10 Error vs iteration curve throughout the optimization process

Table 2 Optimal parameter values for PPR UEL cohesive model

Norm. fracture energy	Tan. fracture energy	Norm. cohesive strength	Tan. cohesive strength	Norm. shape parameter	Tan. shape parameter	Norm. initial slope indicator	Tan. slope indicator
0.1	0.114	4.1	5	4.8	2.36	0.0014	0.0058

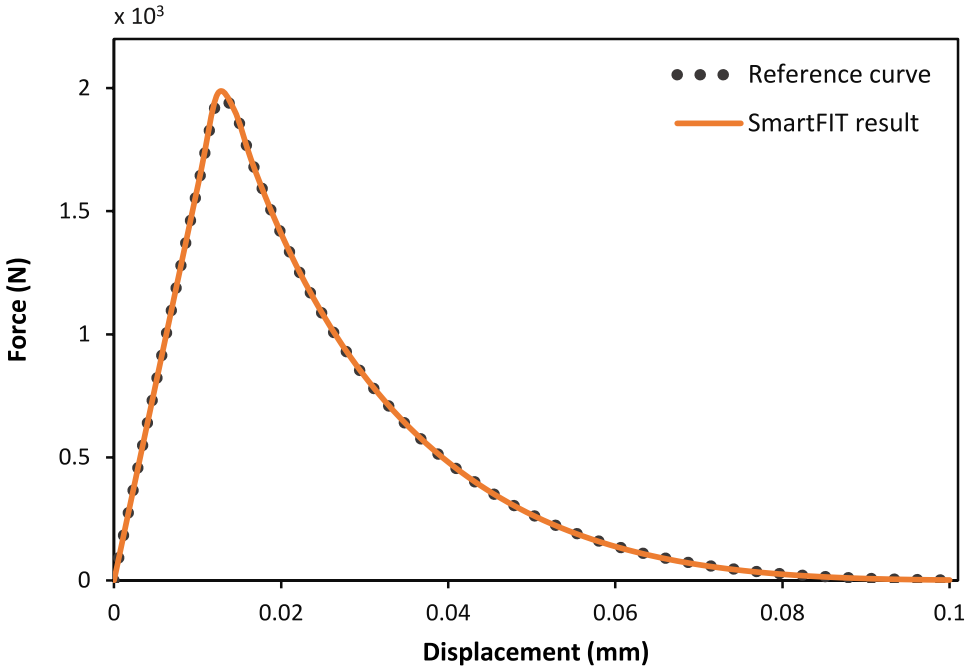


Fig. 11 Comparison of the reference force–displacement curve with results using optimal parameters

correspondence between the two curves. This observation underscores the efficacy of the optimized parameters determined using SmartFIT.

Application 2 – Power-Law Hardening Plasticity Model in UMAT

Theoretical Background

The von Mises model is commonly employed to characterize the behavior of metallic materials. This section provides an overview of conventional von Mises plasticity as outlined by Dunne and Petrinic (2005). This material model assumes small strain plasticity, applicable across both small and large displacement scenarios. According to the classical additive decomposition of strain, the total strain experienced by the material is represented as the sum of elastic (ε^e) and plastic (ε^p) strain tensors, denoted as

$$\varepsilon = \varepsilon^e + \varepsilon^p \tag{15}$$

Therefore, the stress attained at a strain (ε) is determined as

$$\sigma = E\varepsilon^e = E(\varepsilon - \varepsilon^p) \tag{16}$$

The plastic deformation must consistently satisfy the incompressibility condition, implying that deformation occurs without any change in volume. Consequently, the total plastic train rate components amounts to zero, and can be expressed as:+

$$\dot{\varepsilon}^p_{11} + \dot{\varepsilon}^p_{22} + \dot{\varepsilon}^p_{33} = 0 \tag{17}$$

For a given material model, the establishment of a yield condition is necessary to ascertain whether the loading state lies within the elastic or plastic regime. Let f denote a yield function, with $f=0$ serving as the critical criterion. Thus, when the difference between the effective stress (σ_e) and the material yield stress (σ_y) reaches zero, plasticity initiates. This yield function (f) can be mathematically expressed as

$$f = \sigma_e - \sigma_y \tag{18}$$

Several key considerations taken in the von Mises plasticity theory are that (a) the yielding behavior in polycrystalline metals is considered as isotropic. (b) the yielding is not influenced by the hydrostatic stress. and (c) the yield criterion remains consistent regardless of whether the material is under compression or tension. The effective stress that is crucial for determining yielding, is defined based on the distortion energy. This distortion energy, denoted as ψ_d, is a measure of elastic strain energy density's deviatoric component. It is mathematically represented as:

$$\psi_d = \frac{1+\nu}{2E} tr\left((\sigma\prime)^2\right) \tag{19}$$

where $tr\left((\sigma\prime)^2\right)$ denotes the trace of the square of the deviatoric stress tensor ($\sigma\prime$), ν is Poisson's ratio and E is Young's modulus. Using the principal stress

$$\psi_d = \frac{1+\nu}{6E}\left(\left(\sigma_1-\sigma_2\right)^2+\left(\sigma_2-\sigma_3\right)^2+\left(\sigma_3-\sigma_1\right)^2\right) \quad (20)$$

In the context of uniaxial tension, it can be written as

$$\psi_d = \frac{1+\nu}{6E}\sigma_e^2 \quad (21)$$

After re-arranging and substituting this in Eq. (17), the yield function can be formulated as follows,

$$f(\sigma) = \frac{1}{\sqrt{2}}\left[\left(\sigma_1-\sigma_2\right)^2+\left(\sigma_2-\sigma_3\right)^2+\left(\sigma_3-\sigma_1\right)^2\right]^{1/2} - \sigma_y \quad (22)$$

Therefore, the effective stress can be written as follows,

$$\sigma_e = \sqrt{\frac{1}{2}\left[\left(\sigma_1-\sigma_2\right)^2+\left(\sigma_2-\sigma_3\right)^2+\left(\sigma_3-\sigma_1\right)^2\right]} = \sqrt{\frac{3}{2}\sigma\prime : \sigma\prime} = \sqrt{\frac{1}{2}\left[\left(\sigma_{11}-\sigma_{22}\right)^2+\left(\sigma_{22}-\sigma_{33}\right)^2+\left(\sigma_{33}-\sigma_{11}\right)^2+6\sigma_{12}^2+6\sigma_{13}^2+6\sigma_{22}^2\right]} \quad (23)$$

The flow rule is then expressed as a function of the yield function (f) and the plastic multiplier λ as

$$\dot{\varepsilon}^p = \lambda\frac{\partial f}{\partial \sigma} \quad (24)$$

where λ quantifies the magnitude of the plastic strain rate, while $\partial f/\partial\sigma$ provides the direction of the plastic strain increment. An effective plastic strain in the von Mises plasticity is characterized as

$$\varepsilon_p = \sqrt{\frac{2}{3}\varepsilon^p : \varepsilon^p} \quad (25)$$

and accordingly, the plastic flow law is defined as

$$\dot{\varepsilon}^p = \frac{3}{2}\dot{\varepsilon}^p\frac{\sigma\prime}{\sigma_e} \quad (26)$$

The commonly employed formulation of isotropic hardening coupled with a power law hardening rule [26], can be expressed as follows:

$$\sigma_f = \sigma_y\left(1+\frac{E\varepsilon_p}{\sigma_y}\right)^N \quad (27)$$

where $N(0 \le N \le 1)$ represents the strain hardening exponent and σ_f represents the flow stress.

Table 3 Upper and lower bound of UMAT model parameters

	Young's Modulus	Poisson's Ratio	Yield Stress	Strain Hardening
Min. Value	120,000	0.2	400	0.2
Max. Value	360,000	0.4	800	0.6

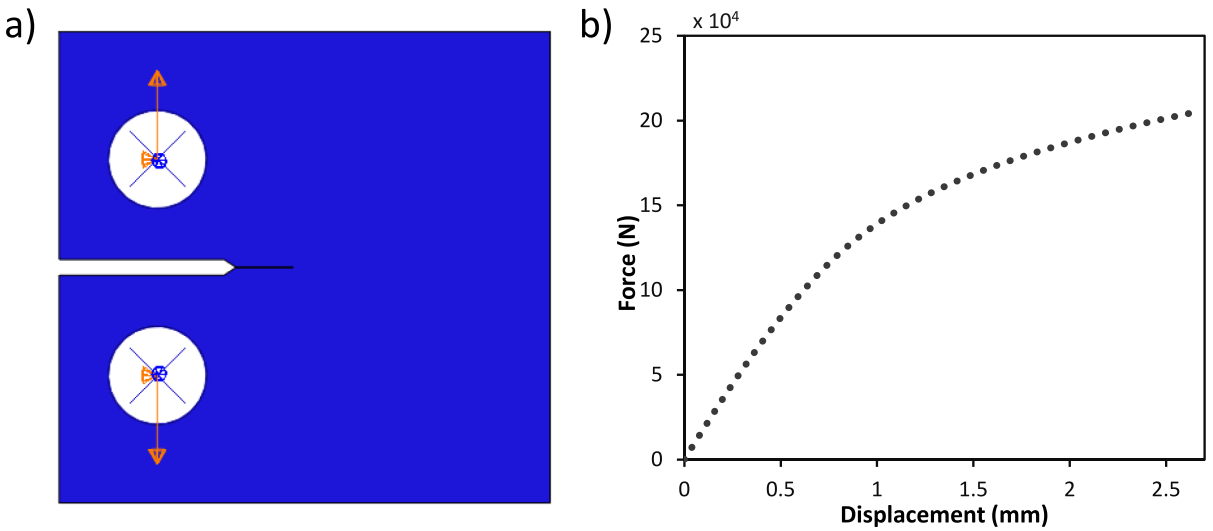


Fig. 12 **a** FE model of compact tension specimen and **b** the reference force–displacement curve

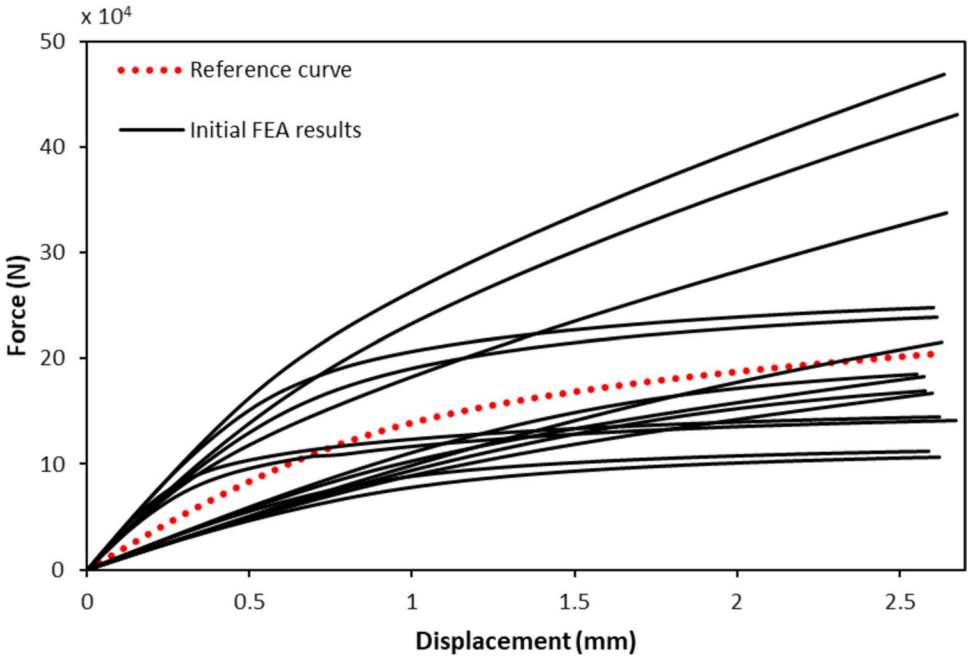


Fig. 13 Comparison of reference force–displacement curve with initial FEA results based on DoE

Problem Definition

In this specific case study, the objective is to determine the parameters of the user material (UMAT) subroutine developed by Martínez-Pañeda et al. [27]. This subroutine facilitates the implementation of classical von Mises plasticity with power law isotropic hardening. Within this UMAT subroutine, four key parameters require accurate identification to effectively define the constitutive behavior. These parameters include Young's modulus, Poisson's ratio, yield stress, and strain hardening exponent. To calibrate these parameters, an FE model of a compact tension test specimen as depicted in Fig. 12 (a), having a width of 62.5 mm and a height of 60 mm is constructed. A displacement loading of 2.5 mm is applied to the holes of the specimen in opposite vertical directions. Given the relatively low number of parameters requiring optimization (four in total), the full factorial method is adopted to design the samples in the DOE.

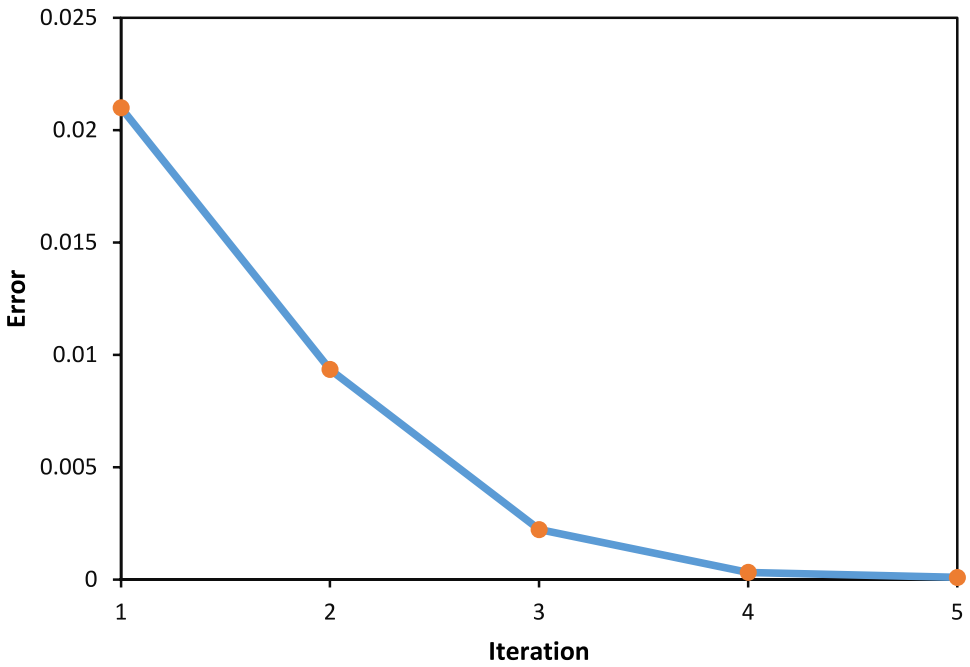


Fig. 14 Error vs iteration curve throughout the optimization process

Table 4 Optimal parameter values for the hardening model

Young's Modulus	Poisson's Ratio	Yield Stress	Strain Hardening
216,675.4	0.21	615.6	0.291

Table 3 outlines the minimum and maximum values for each parameter, guiding the sampling process. Therefore, a total of 2^4 combinations, resulting in 16 unique samples, are generated. Subsequently, finite element analyses are performed for all samples created using the full factorial method. The resulting data is stored in the database for further analysis and ML model training. Figure 13 provides a comparison between the reference curve and the initial FE simulated curves stored in the database. The deviation of the resulting FE curves from the reference curve highlights the inaccuracies in the constitutive parameters employed in the FE model. The ultimate objective is to fit the FE curve to the reference curve by obtaining optimal material parameters through the SmartFIT optimization framework.

Optimization Results

The SmartFIT procedure is initiated to optimize the parameters under consideration. Remarkably, within just five iterations, the calculated error reached below the predefined tolerance threshold, as illustrated in Fig. 14. Again, a gradual decrease in error with each iteration, indicating the iterative refinement process is observed. Specifically, the error computed in the final iteration stands at a mere 0.0002, compared to the initial value of 0.021 recorded in the first increment. This signifies a remarkable reduction of almost 99% in error from its initial value within just five increments. The optimized values of the parameters, presented in Table 4, fall within the predefined upper and lower limits for each parameter. Subsequently, a finite element analysis conducted utilizing these optimal values revealed a striking similarity between the FE result and the reference curve, as depicted in Fig. 15. This close resemblance underscores the accuracy of the optimized parameters in capturing the desired behavior effectively.

Application 3 – Johnson–Cook plasticity model

Theoretical Background

The Johnson–Cook constitutive model, originally proposed by Johnson and Cook [18], has found extensive application in the field of structural analysis. One of its most notable attributes is its simplistic formulation rooted in principles of continuum mechanics and viscoplastic mechanics. At the core of the Johnson–Cook model lies a straightforward mathematical representation of flow stress, which is expressed as the product of three distinct factors: strain hardening $f_1(\varepsilon)$, strain rate hardening $f_2(\dot{\varepsilon})$ and thermal softening $f_3(T)$. This relationship can be expressed as:

$$\sigma_{eq} = f_1(\varepsilon) f_2(\dot{\varepsilon}) f_3(T) \tag{28}$$

The specific form of the equation is as follows [15, 42, 52],

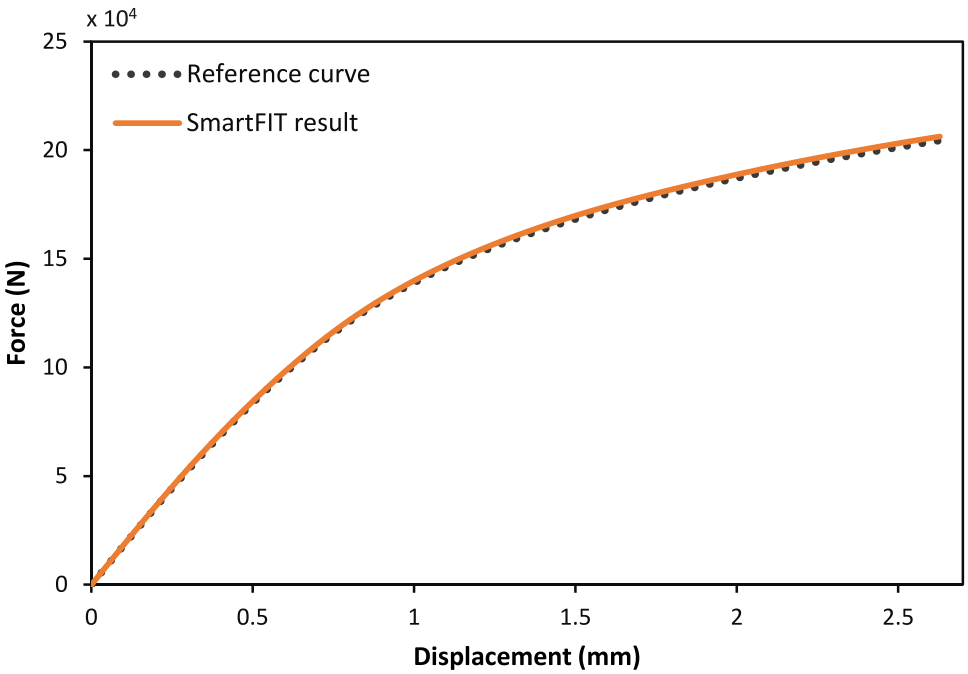


Fig. 15 Comparison of the reference force–displacement curve with results using SmartFIT optimal values

$$\sigma_{eq} = \left(A + B\varepsilon_p^n\right)\left[1 + C\ln\frac{\dot{\varepsilon_p}}{\dot{\varepsilon_0}}\right]\left[1 - \left(\frac{\mathrm{T} - T_0}{T_m - T_0}\right)^m\right] \quad (29)$$

In this equation, σ_{eq} represents the flow stress, ε_p represents the equivalent plastic strain, $\dot{\varepsilon_p}$ represents the plastic strain rate, $\dot{\varepsilon_0}$ represents the reference strain rate, T_0 is a reference temperature and T_m represents the melting temperature. Additionally, A, B, C, n, and m are parameters specific to the material being analyzed. A represents the material's initial yield strength, B and n characterize the material's strain hardening behavior. The parameter C captures the material's sensitivity to strain rate, and m represents the material's sensitivity to thermal effects.

When the deformation temperature is equal to the reference temperature i.e., $T = T_0$, and the deformation strain rate is set to the reference strain rate i.e., $\dot{\varepsilon_p} = \dot{\varepsilon_0} = 1\ \mathrm{s}^{-1}$, Eq. (29) undergoes the following modification:

$$\sigma_{eq} = \left(A + B\varepsilon_p^n\right) \quad (30)$$

This equation provides a relationship between stress and strain. The terms within the second and third sets of brackets in Eq. (29) represent the influences of elevated strain rates and temperature, respectively. In a quasi-static test scenario where, significant thermal changes are absent, the effects described by the second and third factors of the constitutive relationship are typically disregarded. In such cases, only the constants within the first set of brackets need to be determined. Moreover, this plasticity model is often utilized alongside a linear elastic material model, allowing for a comprehensive characterization of material behavior across various loading conditions.

Table 5 The upper and lower bounds of the design parameters

	***E*(MPa)**	***v***	***A*(MPa)**	***B*(MPa)**	***n***
Min. Value	150,000	0.2	300	200	0.2
Max. Value	300,000	0.4	700	800	0.6

Problem Definition

The investigation carried out by Cao et al. [6] involved the examination of X80 pipeline steel under various loading conditions. One aspect of their research involved subjecting dog bone specimens to uniaxial tensile tests, resulting in the generation of force vs. displacement curves, one of which is depicted in Fig. 16. The material exhibits a behavior characterized by both elasticity and strain hardening. The curve in Fig. 16 is used as a reference in this example to determine the parameters of a Johnson–Cook plasticity model. These parameters are initial yield stress (A), the strain hardening constant (B) and the strain hardening exponent (n). Additionally, Young's Modulus (E) and Poisson's ratio (v) also need to be determined to define the material's elastic behavior. A DOE employing a full factorial design was employed to systematically explore the parameter space and optimize these parameters. This methodology facilitated the generation of 32 distinct samples, each characterized by varying combinations of design parameters (A, B, n, E, v). The full factorial DOE method enables a comprehensive evaluation of all linear effects and interactions among the designated parameters, providing a robust understanding of the material's behavior under different conditions. The selection of upper and lower bounds for parameters in a DOE is a

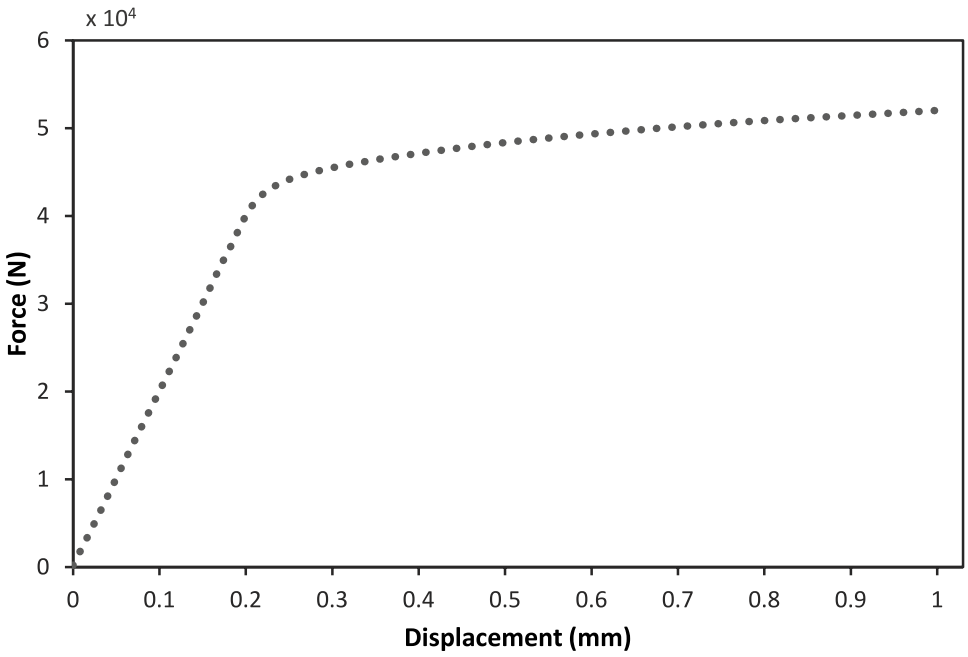


Fig. 16 The reference force–displacement curve obtained by Cao et al. [6]

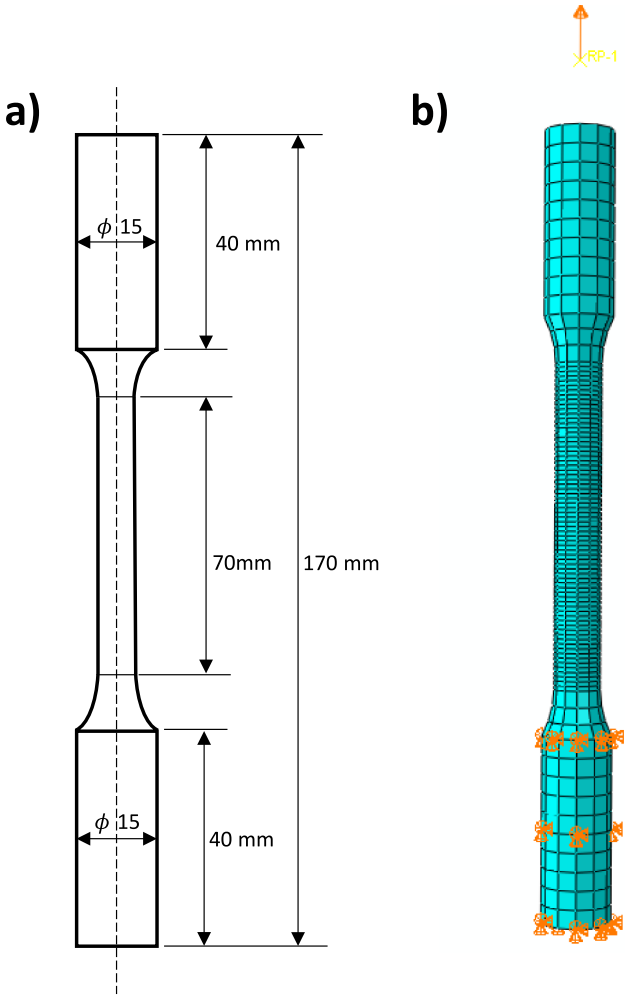


Fig. 17 **a** Dimensions of the tensile bar specimen and **b** its FE model

strategic process that aims at encompassing the range within which optimal values of variable are expected to lie. The bounds established for each variable are outlined in Table 5, guiding the subsequent optimization process towards identifying the most suitable parameter values for modeling the behavior of X80 pipeline steel.

The construction of an FE model was initiated to simulate the experimental specimen, the dimensional specifications of which are presented in Fig. 17 (a). This FE model of a specimen, illustrated in Fig. 17 (b) is utilized for subsequent analyses aimed at optimizing parameter values crucial for characterizing the specimen's behavior. The input file of the FE model was incorporated into SmartFIT, enabling the automatic determination of optimal values. Each sample generated through the DOE approach underwent FE analysis, with the resulting outputs in terms of force vs. displacement data stored within a database. The outcomes of these analyses, depicted in Fig. 18, display a substantial disparity between the reference data and the FE outputs, indicating the utilization of incorrect constitutive model parameters. In response to this disparity, SmartFIT was deployed to utilize the FE output results as training data for machine learning models. Within the SmartFIT framework, the choice between different machine learning models such as ANN and SVR are available. For this example, SVR was deemed appropriate and specific hyperparameters were configured to ensure efficient training. These included setting the kernel to 'rbf', an epsilon value of 0.0001, and a regularization parameter (C) of 5. The remaining hyperparameters were maintained at their default settings. The optimization process, outlined in Sect. "Proposed Machine Learning Based Inverse Methodology", was then initiated, leveraging SmartFIT's capabilities to iteratively refine parameter values towards achieving convergence with the reference data.

Parameter Identification

It took SmartFIT fourteen iterations to reduce the error between FE result and reference curve below the defined tolerance threshold. The iterative reduction in error for each iteration throughout the process is illustrated in Fig. 19. At the end of the second iteration, the error value dropped to 0.0035, showcasing a significant reduction from the initial 0.025 recorded in the first iteration. This remarkable decrease of 86% in error values underscores the substantial progress achieved in refining the accuracy of the process. It's noteworthy that following the sixth iteration, there hasn't been any visible change in the slope of the error curve. This observation suggests that convergence might have been attained earlier, particularly if higher tolerance values had been employed. The optimal values of parameters for the material model obtained at the end of the fourteenth iteration are presented in Table 6. Upon conducting FE analysis of the specimen using the optimized values, it became apparent that the resultant force–displacement curve aligned well with the reference curve, as depicted in Fig. 20. This observation underscores the successful optimization of the Johnson–Cook plasticity model parameters by SmartFIT.

Application 4 – Beam-Column Connection Under Cyclic Loading

To illustrate SmartFIT's robustness, more realistic analysis with complex loading conditions involving a beam-column connection under cyclic loading has been conducted. This example incorporates a more nonlinear loading scenario, where cyclic loading introduces hysteresis in the material behavior. Beam-column connections are critical components in structural systems and accurately modeling their behavior under such nonlinear conditions involves dealing with complex stress–strain relationships. This would better demonstrate SmartFIT's capability to handle real-world, non-linear,

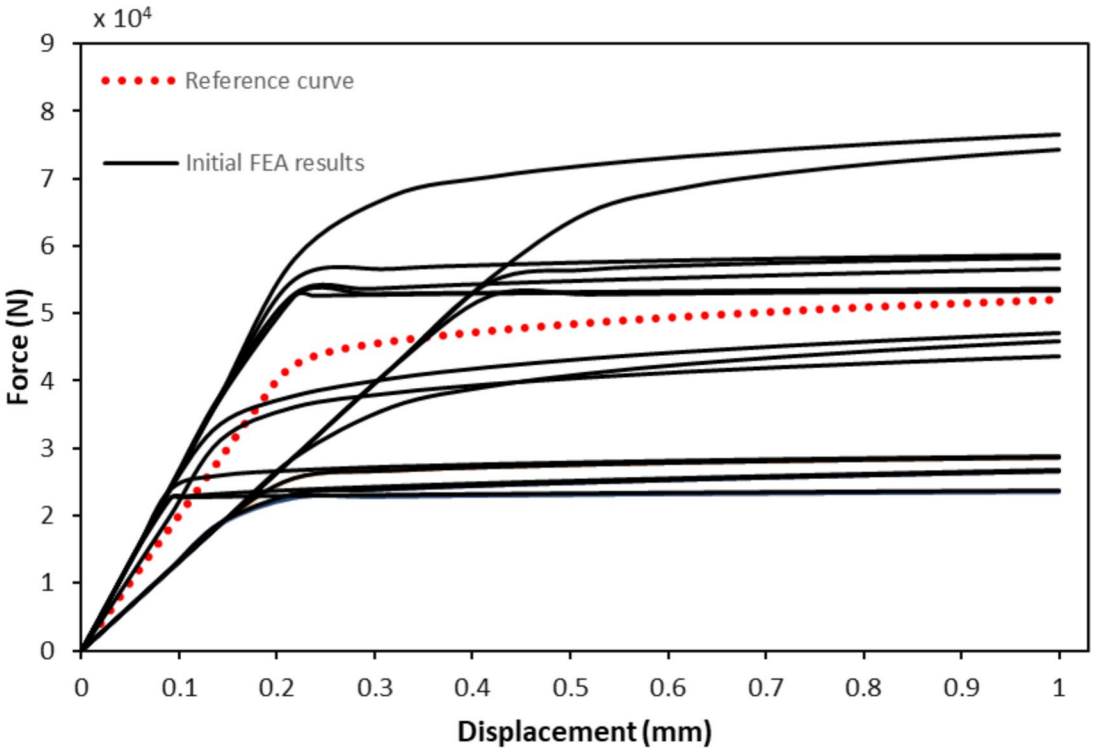


Fig. 18 Comparison of reference force–displacement curve with initial FEA results based on DoE

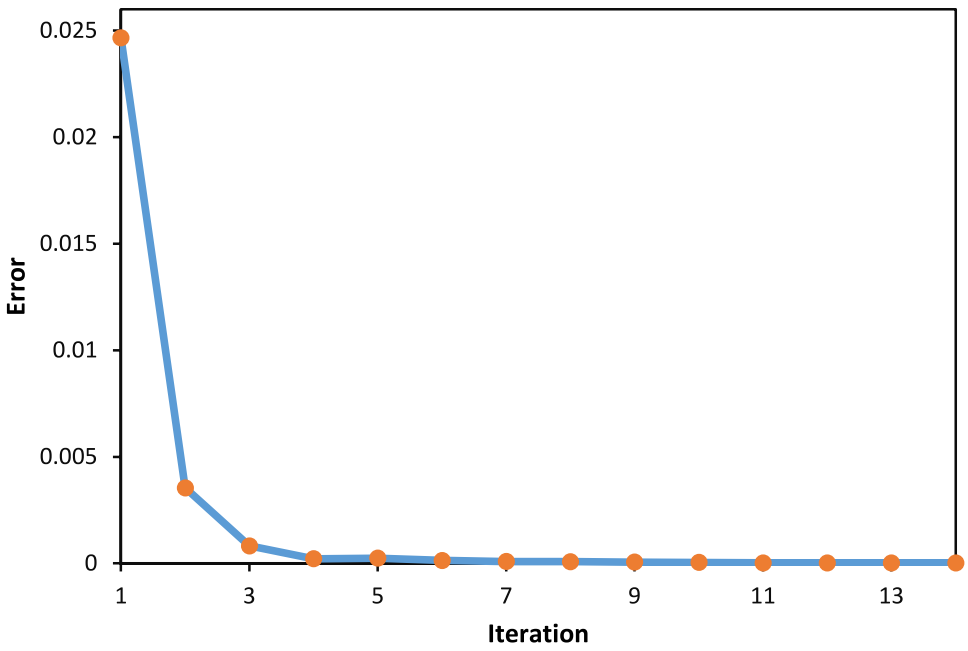


Fig. 19 Error vs iteration curve throughout the optimization process

Table 6 Optimal parameter values for Johnson Cook model

E(MPa)	*v*	*A*(MPa)	*B*(MPa)	*n*
229,169.4	0.25	543	729	0.36

and multiaxial loading conditions. The beam-column connection model adopted in this example is inspired from the experimental work conducted by Swati and Gaurang [47]. They studied the effect of reduced beam section on steel

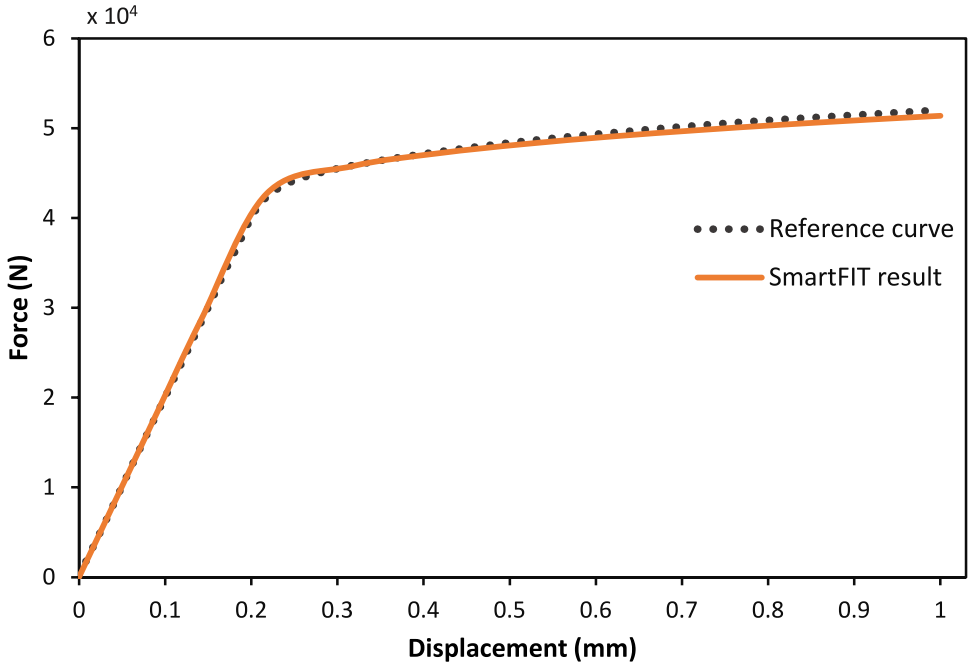


Fig. 20 Comparison of the reference force–displacement curve with results using Smart-FIT optimal values

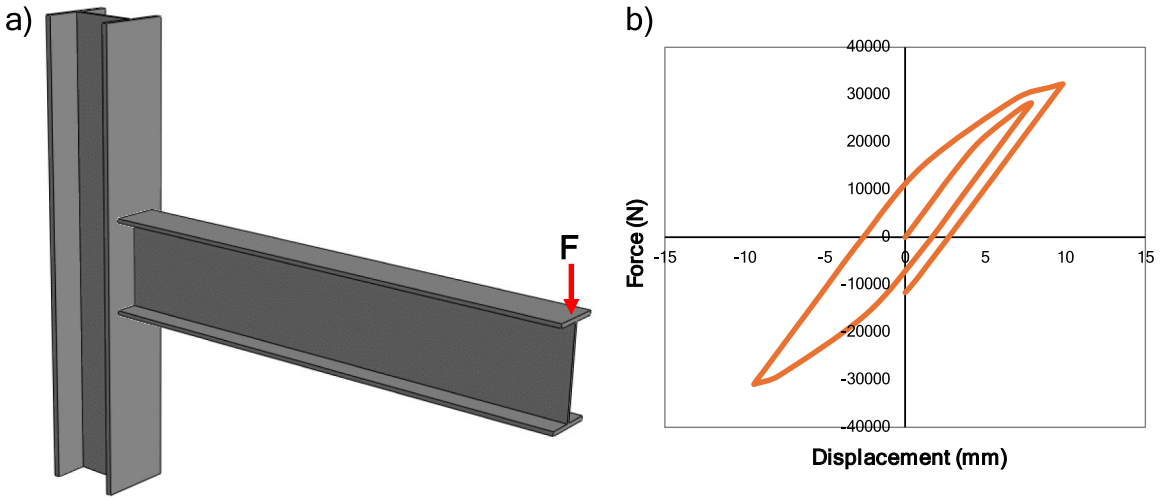


Fig. 21 **A** FE model of a beam-column connection **b** cyclic load applied on the free end of beam

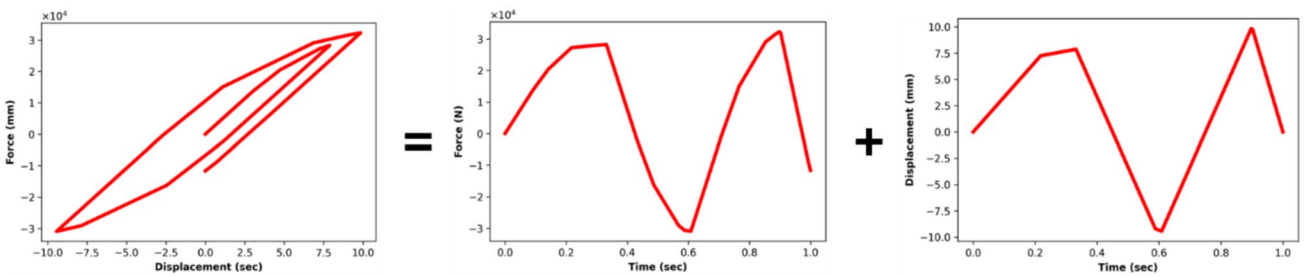


Fig. 22 Cyclic force-displacement hysteresis curves decomposed into force–time and displacement–time curves

Table 7 The upper and lower bounds of the design parameters

	E(MPa)	*v*	*A*(MPa)	*B*(MPa)	*n*
Lower Bound	150,000	0.2	150	300	0.2
Upper Bound	300,000	0.4	300	600	0.6

Table 8 Optimal Johnson-Cook model parameters for the beam-column connection model

E(MPa)	*v*	*A*(MPa)	*B*(MPa)	*n*
196,554.6	0.26	200.9	500	0.42

moment connections under cyclic loading. The FE model of the beam-column connection and the cyclic load applied on the free end of beam is illustrated in Fig. 21.

In a force–displacement plot for cyclic loading, a specific displacement value can correspond to multiple force values due to the hysteresis effect. This complex characteristic makes the force–displacement hysteresis curve challenging for ML models to directly interpret. To overcome this challenge, the hysteresis force–displacement curve is decomposed into force–time and displacement–time curves, as shown in Fig. 22. This decomposition is based on the following considerations:

- In all FE analyses of beam-column connection model, displacement-controlled cyclic loading is applied. This ensures that the displacement–time curve remains the same across all simulations.
- Instead of using the complex force–displacement hysteresis curve, force–time curves are used as the ML model's output. This simplifies the task, as each time point corresponds to a unique force value.

Johnson–Cook plasticity model is used to characterize the nonlinear behavior of the material. This phenomenological constitutive model relies on determination of various parameters to define the material's response. Initially the elastic properties such as Young's modulus (E), Poisson's ratio (v) and plastic parameters for the hardening effects including yield stress (A), hardening constant (B) and hardening exponent (n) are not known. The full factorial design method is used to create every combination of parameter levels using the upper and lower bounds presented in Table 7. This sampling method resulted in the formation of 32 samples, each of which are analyzed for the beam-column connection model using FEA and the corresponding force–time curves are stored in database.

Since the initial samples in DoE are obtained using the min. and max. values of the model parameters, the resulting force–time curves display a substantial difference with the reference curve. SmartFIT is initiated to determine the optimal parameters that produce the structural response similar to one in experimental curve. During the SmartFIT calibration process, the ML model is trained to predict force values at various time points. For this example, the SVR model is selected with an epsilon value of 0.0001 and a regularization parameter of 5. The remaining hyperparameters are maintained at their default settings. The subsequent steps as outlined in Sect. "Proposed Machine Learning Based Inverse Methodology" are carried out leveraging SmartFIT's capabilities to iteratively refine parameter values towards achieving convergence with the reference curve. It took SmartFIT fourteen iterations to reduce the error between FE result and reference curve below the predefined tolerance. The optimal values of parameters for the material model obtained at the end of the fourteenth iteration are presented in Table 8. Upon conducting FE analysis of the beam-column connection model using the optimized parameters, it became apparent that the resultant force–time and displacement–time curves aligned well with their corresponding reference curves. When the force–displacement relationship was reconstructed, it closely matched the reference hysteresis behavior as shown in Fig. 23. This strategy of breaking down the hysteresis behavior into more manageable components enabled SmartFIT to efficiently handle the nonlinear material behavior under cyclic loading.

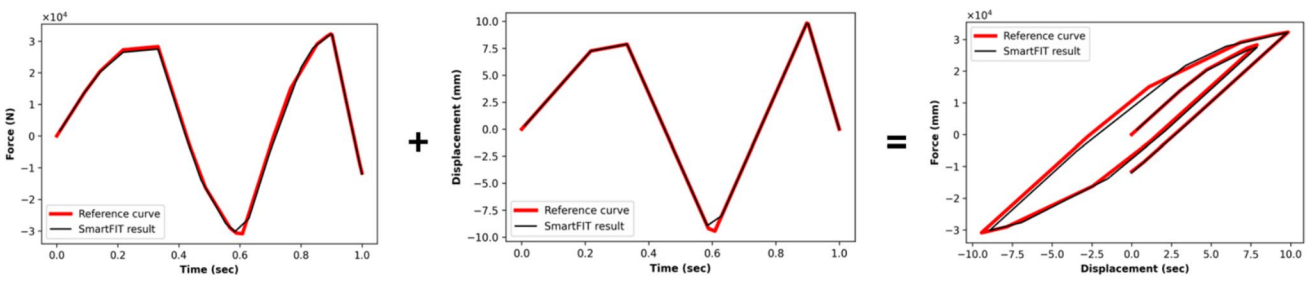


Fig. 23 Comparison of reference curves with the of ones obtained from SmartFIT

Comparison of SmartFIT with Traditional Optimization Method

This section provides a detailed comparison between the SmartFIT method introduced in this paper and traditional optimization approaches. For this purpose, the first two examples presented in Sect. "Application 1 - UEL implementation of cohesive zone model" and Sect. "Application 2 – Power-law hardening plasticity model in UMAT" focusing on determining the parameters of the UEL and UMAT models are solved using a traditional optimization algorithm based on the least squares method. The objective function for this optimization algorithm is formulated to calculate the sum of squared differences between the simulation results and the experimental data. Unlike SmartFIT, this method does not involve the construction of a simulation database through Design of Experiments (DoE) or the utilization of any machine learning (ML) models. Instead, the optimization process is initiated by an initial guess of the parameters, iteratively adjusting these values to minimize the error between the simulation and experimental results. To ensure consistency, the same Nelder-Mead method used by SmartFIT is applied here for comparison. The upper and lower bounds of the parameters are set identical to those selected for SmartFIT. The stopping criteria, which terminates the optimization process once the error between the simulation and experimental data reaches a predefined tolerance, is also kept consistent between the two approaches. To prevent the optimization process from running indefinitely or stopping prematurely, the maximum function evaluation and function tolerance values are selected as 1000 and 0.0001, respectively.

In the following sections, a detailed analysis of the parameter identification results obtained for both the UEL and UMAT models using the traditional optimization method is provided. These results are compared with the outcomes generated by SmartFIT to illustrate the efficiency and accuracy of each approach. Specifically, the computational time and the quality of the fit between the simulation and experimental data for both methods are highlighted.

UEL cohesive zone model

In this subsection, the traditional optimization method to identify the eight parameters of the PPR potential-based cohesive zone model implemented within the UEL framework is applied. The optimization process required a total of 503 function evaluations to minimize the error between the simulated and reference force–displacement curves to below the specified tolerance level. This approach proved to be computationally expensive as each function evaluation requires an FE simulation. In total, the traditional optimization method took 106 min to converge and yield optimal parameters for the UEL model. The resulting force–displacement curve demonstrated very good agreement with the reference curve.

On the other hand, SmartFIT required 64 initial FE simulations from the DoE to train the ML model. An additional 28 FE simulations were then executed during the optimization process, resulting in a total of 92 simulations. The force–displacement curve obtained from SmartFIT closely matched the results from the traditional optimization method. However, SmartFIT achieved this result in just 35 min. Specifically, the initial FE simulations took 24 min and the parameter identification during the optimization process took 11 min.

The convergence behavior of both optimization methods is illustrated in Fig. 24, which shows the error versus iteration curves on a logarithmic scale. This log scale provides better insight into the optimization process by making incremental improvements more visible, especially during the

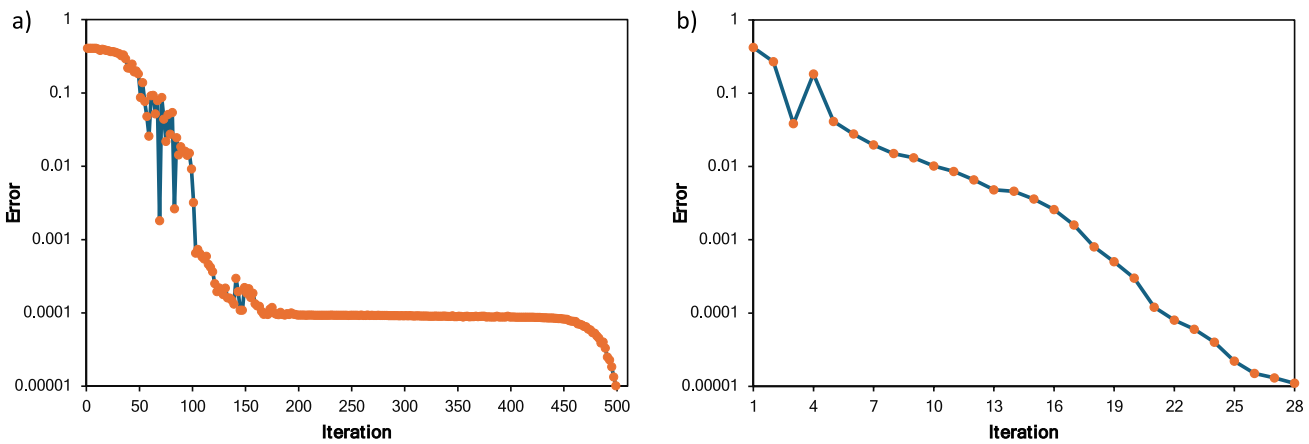


Fig. 24 Error vs iteration curve for a) traditional optimization method and b) SmartFIT optimization

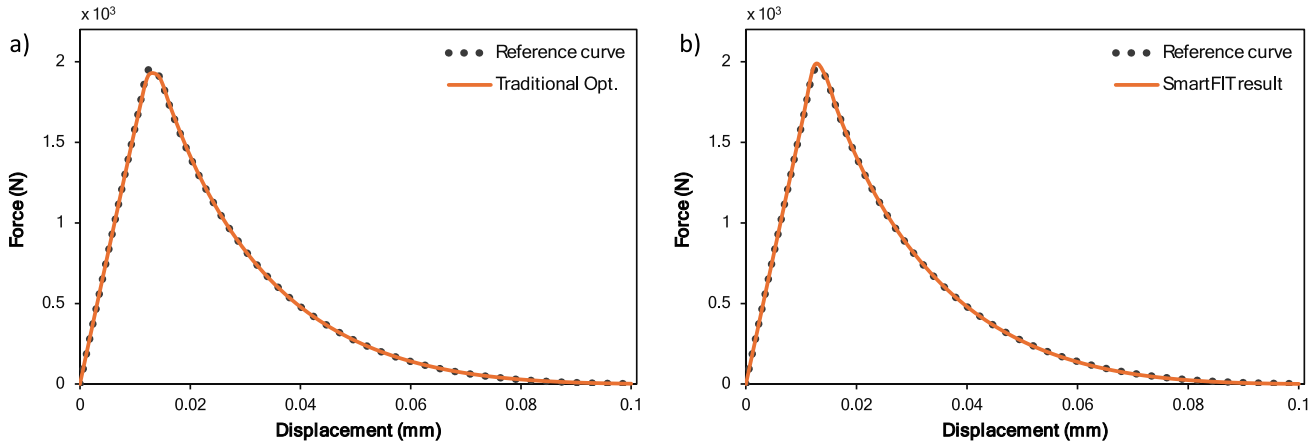


Fig. 25 Comparison of force–displacement reference curves with the of ones obtained from a) traditional optimization and b) SmartFIT result

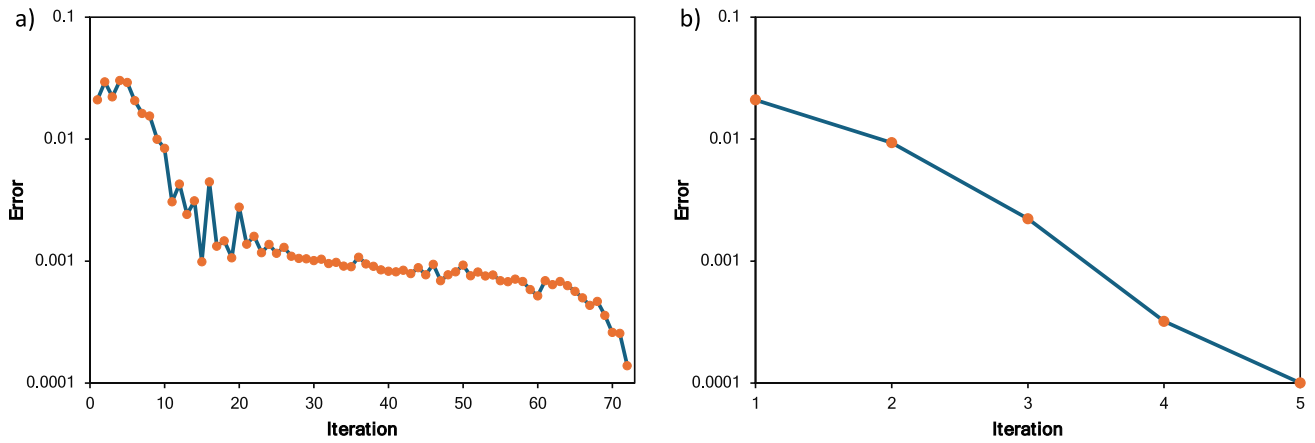


Fig. 26 Error vs iteration plot for **a** traditional optimization and **b** SmartFIT optimization

later stages when errors are very small. Figure 25 compares the force–displacement curves obtained using the optimal parameters from both the traditional method and SmartFIT. As evident from these figures, although both methods produce similar results in terms of accuracy, SmartFIT is far more efficient. SmartFIT is not only approximately three times faster than the traditional optimization method but also requires around five times fewer FE simulations to achieve the same level of accuracy.

UMAT hardening model

In this example, the traditional optimization method to identify four key parameters that characterize the isotropic power-law hardening plasticity model within the UMAT framework is applied. The objective function is evaluated 72 times during the optimization process to reduce the error between the reference and simulated force–displacement curves below a specified tolerance. This traditional optimization process took 52 min to converge to an optimal solution. After identifying the optimal set of parameters, these values were used to perform FE analysis, and the resulting force–displacement curve showed excellent alignment with the reference curve.

For the same parameter identification problem, SmartFIT demonstrated a more efficient process. A total of 22 FE simulations were conducted throughout the process. Out of these, 17 simulation pertains to initial FE analysis used to train the ML model, while the remaining 5 simulations were executed during the optimization phase. SmartFIT completed the entire optimization process in just 25 min in which the first 19 min was utilized for initial FE analyses and an additional 6 min for parameter identification.

Figure 26 presents the error versus iteration curves for both the traditional optimization method and SmartFIT. Additionally, the force–displacement curves obtained from

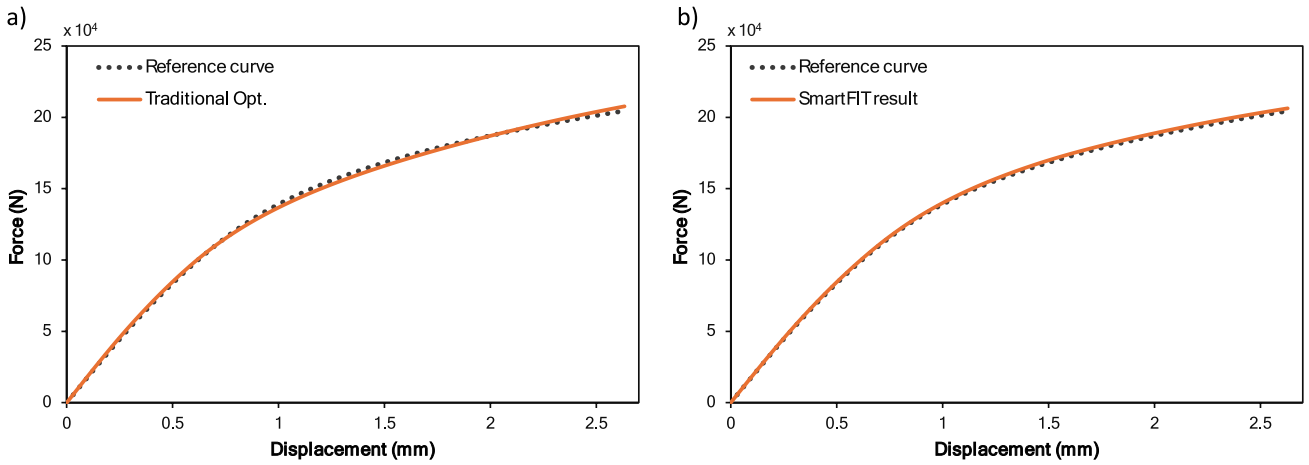


Fig. 27 Comparison of force–displacement reference curves with results from a) traditional optimization and b) SmartFIT optimization

each approach using the respective optimal parameters are compared in Fig. 27. As seen in both figures, the final results in terms of accuracy are similar for both methods. However, SmartFIT proves to be significantly more efficient by taking about half the time of the traditional method and requiring only one-third of the FE simulations. This highlights the superior computational efficiency for parameter optimization in the UMAT model.

Conclusion

This article presents an inverse methodology termed SmartFIT for parameter identification in material constitutive models used in FE simulations. The framework of this methodology systematically integrates ML techniques such as ANN and SVR with optimization algorithms utilizing hybrid numerical-experimental data. The primary objective of SmartFIT is to streamline the model calibration process by reducing computational time while ensuring accurate parameter identification. The effectiveness of methodology has been demonstrated through a series of examples. In the first example, the characterization of cohesive zone models implemented in UEL was successfully carried out by determining its eight governing parameters. In the second example, four parameters required for defining the material's hardening behavior in UMAT were identified. The third example involved the calibration of five parameters for the Johnson–Cook plasticity model. In all cases, SmartFIT identified parameters that led to accurate simulation results closely matching experimental observations. A more complex beam-column connection model subjected to cyclic loading was also analyzed to demonstrate the robustness of SmartFIT. The methodology successfully identified the optimal parameters even under challenging hysteresis-based loading conditions. Furthermore, SmartFIT's performance was compared with traditional optimization methods for parameter identification. The results showed that although both methods achieved similar curve-fitting accuracy, SmartFIT is considerably more efficient, as it reduced computational time by 2–3 times. The computational in SmartFIT time can be further reduced by adjusting the predefined tolerance level, though this will come at the cost of reduced accuracy.

Acknowledgements Authors would like to thank Bursa Uludağ University, Scientific Research Projects (BAP) (Project No: FGA-2022-1211) for their support and the scholarship they provided to the first author.

Funding Bursa Uludağ University Scientific Research Projects (BAP) (Project No: FGA-2022–1211) funded the first author during the course of this work. The authors are grateful for this support.

Data Availability Some or all data that support this study's findings are available from the corresponding author upon reasonable request.

Declarations

Ethical Approval Not applicable.

Conflict of Interest The authors declare that they have no conflict of interest.

References

1. Andrade-Campos A, Bastos N, Conde M, Gonçalves M, Henriques J, Lourenço R, ... & Rumor L (2022, May). On the inverse identification methods for forming plasticity models using full-field measurements. In IOP Conference Series: Materials Science and Engineering (Vol. 1238, No. 1, p. 012059). IOP Publishing.

2. Barlat F, Brem JC, Yoon JW, Chung K, Dick RE, Lege DJ, Chu E (2003) Plane stress yield function for aluminum alloy sheets—part 1: theory. Int J Plast 19(9):1297–1319
3. Blaysat B, Florentin E, Lubineau G, Moussawi A (2012) A Dissipation Gap Method for full-field measurement-based identification of elasto-plastic material parameters. Int J Numer Meth Eng 91(7):685–704
4. Bonnet M, Constantinescu A (2005) Inverse problems in elasticity. Inverse Prob 21(2):R1
5. Burhenne, S., Jacob, D., & Henze, G. P. (2011, November). Sampling based on Sobol'sequences for Monte Carlo techniques applied to building simulations. In Proc. Int. Conf. Build. Simulat (pp. 1816–1823).
6. Cao Y, Zhen Y, Song M, Yi H, Li F, Li X (2020) Determination of Johnson-Cook parameters and evaluation of Charpy impact test performance for X80 pipeline steel. Int J Mech Sci 179:105627
7. Chemisky Y, Meraghni F, Bourgeois N, Cornell S, Echchorfi R, Patoor E (2015) Analysis of the deformation paths and thermomechanical parameter identification of a shape memory alloy using digital image correlation over heterogeneous tests. Int J Mech Sci 96:13–24
8. Claire D, Hild F, Roux S (2004) A finite element formulation to identify damage fields: the equilibrium gap method. Int J Numer Meth Eng 61(2):189–208
9. Cooreman S, Lecompte D, Sol H, Vantomme J, Debruyne D (2008) Identification of mechanical material behavior through inverse modeling and DIC. Exp Mech 48:421–433
10. Dige N, Diwekar U (2018) Efficient sampling algorithm for large-scale optimization under uncertainty problems. Comput Chem Eng 115:431–454
11. Estrin Y, Mecking H (1984) A unified phenomenological description of work hardening and creep based on one-parameter models. Acta Metall 32(1):57–70
12. Fayad SS, Jones EMC, Seidl DT, Reu PL, Lambros J (2023) On the importance of direct-levelling for constitutive material model calibration using Digital Image Correlation and finite element model updating. Exp Mech 63(3):467–484
13. Gambirasio L, Rizzi E (2016) An enhanced Johnson-Cook strength model for splitting strain rate and temperature effects on lower yield stress and plastic flow. Comput Mater Sci 113:231–265
14. Grédiac, M. (1989). Principe des travaux virtuels et identification. Comptes rendus de l'Académie des sciences. Série 2, Mécanique, Physique, Chimie, Sciences de l'univers, Sciences de la Terre, 309(1), 1–5.
15. He A, Xie G, Zhang H, Wang X (2013) A comparative study on Johnson-Cook, modified Johnson-Cook and Arrhenius-type constitutive models to predict the high temperature flow stress in 20CrMo alloy steel. Mater Des 1980–2015(52):677–685
16. Hollomon JH (1945) Tensile deformation. Aime Trans 12(4):1–22
17. Johnson, G. R. (1983). A Constitutive Model and Date for Metals Subject to Large Strains, High Strain Rate and High Temperatures. In Proc. of 7th Int. Symp. on Ballistics, The Hague.
18. Johnson, G.R, Cook, WHA (1983) Constitutive model and data for metals subjected to large strains, high strain rates and high temperatures. In Proceedings of the 7th International Symposium on Ballistics vol. 21, The Netherlands, pp. 541–547
19. Kavanagh KT, Clough RW (1971) Finite element applications in the characterization of elastic solids. Int J Solids Struct 7(1):11–23
20. Kim H, Yoon JW, Chung K, Lee MG (2020) A multiplicative plastic hardening model in consideration of strain softening and strain rate: Theoretical derivation and characterization of model parameters with simple tension and creep test. Int J Mech Sci 187:105913
21. Ladeveze P, Leguillon D (1983) Error estimate procedure in the finite element method and applications. SIAM J Numer Anal 20(3):485–509
22. Lin DK, Simpson TW, Chen W (2001) Sampling strategies for computer experiments: design and analysis. Int J Relia Appl 2(3):209–240
23. Ludwik P, in: Julius (Ed.), Element der Tech. Mech., Springer, Berlin (1909) pp. 32.
24. Makhool L, & Balzani D (2024). Unique Identification of Stiffness Parameters in Hyperelastic Models for Anisotropic, Deformable, Thin Materials Based on a Single Experiment-A Feasibility Study Based on Virtual Full-Field Data. Experimental Mechanics, 1–23.
25. Markiewicz É, Langrand B, Notta-Cuvier D (2017) A review of characterisation and parameters identification of materials constitutive and damage models: From normalised direct approach to most advanced inverse problem resolution. Int J Impact Eng 110:371–381
26. Martínez-Pañeda E, Niordson CF (2016) On fracture in finite strain gradient plasticity. Int J Plast 80:154–167
27. Martínez-Pañeda E, Fuentes-Alonso S, Betegón C (2019) Gradient-enhanced statistical analysis of cleavage fracture. Eur J Mech-A/Solids 77:103785
28. Martins JMP, Andrade-Campos A, Thuillier S (2018) Comparison of inverse identification strategies for constitutive mechanical models using full-field measurements. Int J Mech Sci 145:330–345
29. Moussawi A, Lubineau G, Florentin E, Blaysat B (2013) The constitutive compatibility method for identification of material parameters based on full-field measurements. Comput Methods Appl Mech Eng 265:1–14
30. Nsengiyumva G, Kim YR (2022) Field Displacement-Based Inverse Method for Elastic and Viscoelastic Constitutive Properties. Exp Mech 62(9):1553–1568
31. Park K, Paulino GH (2012) Computational implementation of the PPR potential-based cohesive model in ABAQUS: Educational perspective. Eng Fract Mech 93:239–262
32. Park K, Paulino GH, Roesler JR (2009) A unified potential-based cohesive model of mixed-mode fracture. J Mech Phys Solids 57(6):891–908
33. Pierron F, & Grédiac M (2021). Towards Material Testing 2.0. A review of test design for identification of constitutive parameters from full-field measurements. Strain, 57(1), e12370.
34. Ponthot JP, Kleinermann JP (2006) A cascade optimization methodology for automatic parameter identification and shape/process optimization in metal forming simulation. Comput Methods Appl Mech Eng 195(41–43):5472–5508
35. Pottier T, Toussaint F, Louche H, Vacher P (2013) Inelastic heat fraction estimation from two successive mechanical and thermal analyses and full-field measurements. Eur J Mech-A/Solids 38:1–11
36. Prates PA, Pereira AFG, Sakharova NA, Oliveira MC, Fernandes JV (2016). Inverse strategies for identifying the parameters of constitutive laws of metal sheets. Advances in Materials Science and Engineering, 2016.
37. Renardy M, Joslyn LR, Millar JA, Kirschner DE (2021) To Sobol or not to Sobol? The effects of sampling schemes in systems biology applications. Math Biosci 337:108593
38. Réthoré J (2010) A fully integrated noise robust strategy for the identification of constitutive laws from digital images. Int J Numer Meth Eng 84(6):631–660
39. Roux É, & Bouchard PO (2010). Ductile damage material parameter identification: numerical investigation. In Tenth International Conference on Computational Structures Technology (No. 93, pp. Paper-135). Civil-Comp Press.
40. Roux E, Bouchard PO (2015) On the interest of using full field measurements in ductile damage model calibration. Int J Solids Struct 72:50–62

41. Saltelli A, Annoni P, Azzini I, Campolongo F, Ratto M, Tarantola S (2010). Variance based sensitivity analysis of model output. Design and estimator for the total sensitivity index. Comput Phys Commun, 181(2), 259–270.
42. Samantaray D, Mandal S, Bhaduri AK (2009) A comparative study on Johnson Cook, modified Zerilli-Armstrong and Arrhenius-type constitutive models to predict elevated temperature flow behavior in modified 9Cr–1Mo steel. Comput Mater Sci 47(2):568–576
43. Santiago J, Claeys-Bruno M, Sergent M (2012) Construction of space-filling designs using WSP algorithm for high dimensional spaces. Chemom Intell Lab Syst 113:26–31
44. Springmann M, Kuna M (2005) Identification of material parameters of the Gurson–Tvergaard–Needleman model by combined experimental and numerical techniques. Comput Mater Sci 33(4):501–509
45. Sun C, Lin QL, Chen JB (2022) An Inverse Identification Method for the Characterization of Elastic Conforming Contact Behavior During Flat Punch Indentation. Exp Mech 62(5):745–759
46. Sung JH, Kim JH, Wagoner RH (2010) A plastic constitutive equation incorporating strain, strain-rate, and temperature. Int J Plast 26(12):1746–1771
47. Swati AK, Gaurang V (2014) Study of steel moment connection with and without reduced beam section. Case Stud Struct Eng 1:26–31
48. Tariq A, Uzun B, Deliktaş B, Yaylı MÖ (2023). Assessment of machine learning methods predicting the axial vibration frequencies of microbars. ZAMM-Journal of Applied Mathematics and Mechanics/Zeitschrift für Angewandte Mathematik und Mechanik, e202300916.
49. Voce E (1948) The relationship between stress and strain for homogeneous deformation. J Inst Met 74:537–562
50. Wang X, Huang C, Zou B, Liu H, Zhu H, Wang J (2013) Dynamic behavior and a modified Johnson-Cook constitutive model of Inconel 718 at high strain rate and elevated temperature. Mater Sci Eng, A 580:385–390
51. Yun GJ, Shang S (2011) A self-optimizing inverse analysis method for estimation of cyclic elasto-plasticity model parameters. Int J Plast 27(4):576–595
52. Zhan H, Wang G, Kent D, Dargusch M (2014) Constitutive modelling of the flow behaviour of a β titanium alloy at high strain rates and elevated temperatures using the Johnson-Cook and modified Zerilli-Armstrong models. Mater Sci Eng, A 612:71–79

Publisher's Note Springer Nature remains neutral with regard to jurisdictional claims in published maps and institutional affiliations.

Springer Nature or its licensor (e.g. a society or other partner) holds exclusive rights to this article under a publishing agreement with the author(s) or other rightsholder(s); author self-archiving of the accepted manuscript version of this article is solely governed by the terms of such publishing agreement and applicable law.